Dissertation

submitted to the

Combined Faculties for the Natural Sciences and for Mathematics

of the Ruperto-Carola University of Heidelberg, Germany

for the degree of

Doctor of Natural Sciences

Presented by

M.Sc. Yan Shi

Born in: Shandong, China

Oral-examination: June 23rd, 2015

Regulation of Adult Neural Stem Cell Activation by Orphan Nuclear Receptor TLX (NR2E1) and Notch Signaling

Referees:

Prof. Dr. Hilmar Bading

Prof. Dr. Ulrike Müller

Table of Contents

Summary

The adult mammalian brain contains neural stem cells (NSCs) that continue to generate neurons throughout adulthood, a process referred to as neurogenesis. Adult NSCs are relatively quiescent and undergo cell division only when they are activated to reenter the cell cycle. Two types of quiescent NSCs have been previously identified, which can be distinguished on the basis of differential expression of Prominin-1 (Pro). Upon activation and asymmetrical division, a NSC self-renews and gives rise to a transit-amplifying precursor (TAP), which will rapidly divide while differentiating into neuroblasts. Our group has developed an approach based on fluorescence activated cell sorting (FACS) to purify quiescent NSCs (qNSCs), activated NSCs (aNSCs) and TAPs.

We have previously shown that in adult NSCs the orphan nuclear receptor Tailless (*Tlx*, NR2E1) is essential for promoting cell cycle entry and the transition from qNSCs to aNSCs. Therefore, mice lacking *Tlx* expression ($Tlx^{-/-}$) represent a nice model system to investigate the mechanisms underlying NSC activation. To further understand the molecular mechanisms underlying the effect of TLX on NSC activation I have compared gene expression in NSCs isolated from wild type (WT) and $Tlx^{-/-}$ mice. This analysis revealed an upregulation of *Hes1* expression and a significant change in the expression of several genes associated to the Notch pathway in both Pro^{+} and Pro^{-} mutant qNSCs. Moreover, in the absence of TLX, the nuclear localization of the Notch intracellular domain (NICD) was increased in Pro^{-} qNSCs, suggesting hyper activation of the canonical Notch pathway, which may prevent cell cycle entry. To provide support for this hypothesis, I have investigated the effect of pharmacological inhibition of Notch signaling on NSC activation. These experiments revealed that indeed blockade of Notch signaling increased proliferation of both WT and $Tlx^{-/-}$ precursors. They also showed that inhibition of Notch signaling leads to the generation of Pro^{+} qNSCs from the Pro^{-} cell pool, suggesting a lineage relationship between the two groups of qNSCs. Since TLX is a transcriptional repressor, it may modulate Notch signaling by repressing the expression of *Hes1*. To further investigate this hypothesis I have taken advantage of luciferase and chromatin immunoprecipitation (ChIP) assays and I was able to show that TLX represses *Hes1* expression and that this effect requires the presence of the RBPJ binding site.

Taken together, my results have uncovered a previously unknown function of TLX in the regulation of *Hes1* expression, which affects the activation of the canonical Notch pathway in NSCs and also the progression from Pro^{-} to Pro^{+} qNSCs.

Zusammenfassung

Das adulte Säugetiergehirn enthält neurale Stammzellen (NSCs), die lebenslang Nervenzellen bilden, ein Prozess, den man als Neurogenese bezeichnet. Die adulten NSCs befinden sich meist im ruhenden Zustand und teilen sich nur nach Aktivierung, um erneut in den Zellteilungszyklus zu treten. Kürzlich wurden zwei Typen von ruhenden NSCs identifiziert, die man aufgrund der unterschiedlichen Prominin-1 (Pro) Expression unterscheiden kann. Nach Aktivierung und asymmetrischer Zellteilung erneuert sich die NSC selbst, und es entsteht jeweils eine NSC und eine Transit-Amplifying-Precursorzelle (TAP), die sich schnell weiterteilt und in Neuroblasten differenziert.

Unsere Arbeitsgruppe hat eine Methode entwickelt, die auf der Fluoreszenz aktivierten Zellsortierung (FACS) beruht, um ruhende NSCs (rNSCs), aktivierte NSCs (aNSCs) und TAPs aufzureinigen. Wir haben kürzlich gezeigt, dass in adulten NSCs der Orphan-Nukleare-Rezeptor Tailless (TLX, NR2E1) essentiell ist für die Einleitung des Zellzyklus und den Übergang von rNSCs zu aNSCs. Die *Tlx* knockout (*Tlx*$^{-/-}$) Maus stellt deshalb ein interessantes Model zur Untersuchung von Mechanismen der NSCs Aktivierung dar. Um zu verstehen, welche molekularen Mechanismen dem Effekt von TLX bei der NSC Aktivierung zugrunde liegen, habe ich die Genexpression isolierter NSCs in Wildtyp (WT) und *Tlx*$^{-/-}$ Mäusen verglichen. Diese Analysen haben eine Hochregulierung der *Hes1* Expression und eine signifikante Expressionsänderung verschiedener mit dem Notch Signalweg assoziierter Gene, sowohl in Pro^{+} als auch in Pro^{-} mutierten rNSCs nachgewiesen. Darüberhinaus war bei Abwesenheit von TLX die Kernlokalisierung der Notch intrazellulären Domäne (NICD) in Pro^{-} rNSCs erhöht. Dies deutet auf eine Hyperaktivierung des kanonischen Notch Signalweges hin, die den Eintritt in den Zellzyklus verhindert. Um diese Hypothese zu überprüfen, habe ich den Effekt der pharmakologischen Blockierung von Notch auf die NSC Aktivierung untersucht. Durch die Blockierung des Notch Signalweges zeigten die Experimente tatsächlich eine Proliferationszunahme sowohl in WT als auch in *Tlx*$^{-/-}$ Vorläuferzellen. Ich konnte ebenfalls zeigen, dass durch die Inhibierung von Notch Pro^{+} rNSCs aus dem Pro^{-}Zellpool entstehen, was auf eine “lineage relationship” schließen lässt. Da TLX als Transkriptionsrepressor fungiert, kann es durch Herunterregulierung der *Hes1* Expression Notch Signaling beeinflussen. Zur weiteren Untersuchung dieser Fragestellung habe ich Luziferase und Chromatin-Immunopräzipitations (ChIP) Assays eingesetzt und konnte nachweisen, dass TLX die Expression von *Hes1* unterdrückt, wobei eine RBPJ Bindungsstelle notwendig ist.

Zusammenfassend zeigen meine Ergebnisse eine bisher unbekannte Funktion von TLX bei der Regulation der *Hes1* Expression, welche die Aktivierung des kanonischen Notch Signalweges in NSCs und den Übergang von Pro^{-} zu Pro^{+} rNSCs beeinflusst.

1. Introduction

1.1 Neurogenesis in the adult brain

Stem cells are characterized by their capability for self-renewal and differentiation into multiple cell types (multi-potency). Neural stem cells (NSCs) generate the main cell types of nervous system, i.e. neurons, astrocytes and oligodendrocytes.

The generation of new neurons is most active during embryonic and neonatal development. However, new neurons are continuously generated throughout adulthood, a process called neurogenesis (Altman, 1962). In the mammalian brain neurogenesis mainly occurs in two regions: the subgranular zone (SGZ) of the hippocampus and the subventricular zone (SVZ) of the lateral ventricles (Figure 1.1).

Figure 1.1 Adult neurogenesis in the mammalian brain. The two neurogenic regions in the brain: the subventricular zone (SVZ) of lateral ventricles (LV) and the subgranular zone (SGZ) of dentate gyrus (DG) in the hippocampus. The Neural progenitor cells of SVZ migrate to the olfactory bulb (OB) through the rostral migratory stream (RMS) and differentiate into interneurons. The NSCs in the DG of the hippocampus generate granule neurons. A: anterior; V: ventral (Cartoon adapt from Fischer et al., 2011)

1.2 Adult neural stem cell niche in subventricular zone

The division and differentiation of NSCs are controlled by the microenvironment (niche). The neurogenic niche of the SVZ is composed by multiple elements, including cells, blood vessel and the cerebrospinal fluid (CSF) (Ihrie and Avarez-Buylla, 2011). As illustrated in Figure 1.2, the apical side of the NSCs contacts the ventricle and basal side the blood vessels. The ependymal cells that are located at the apical side of the SVZ provide a barrier between the niche and the CSF. The motile cilia of the ependymal cells maintain the flow of the CSF in the ventricle and express at the tip the membrane glycoprotein Prominin-1. The apical membranes

of ependymal cells and NSCs form a pinwheel-like structure with NSCs occupying the center of the pinwheel. Most adult NSCs are quiescent and extend a primary cilium into the ventricle. Upon activation and entry into the cell cycle NSCs retract the primary cilium. Upon cell division NSCs give rise to transit amplifying progenitors (TAPs), which are also referred to as type C cells. Unlike NSCs, TAPs proliferate very rapidly and form intermediate progenitors which progressively differentiate into neuroblasts (type A cells).

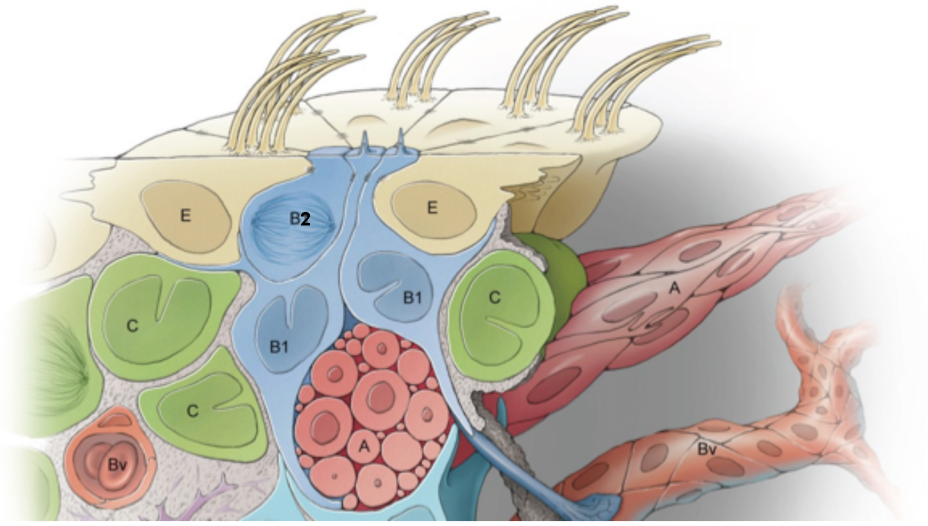

Figure 1.2 Schematic illustration of coronary section of adult neural stem cell niche in SVZ. The top is the apical side of ventricle. The Ependymal (E, beige) cells are multiciliated and have motile cilia that can propel the cerebrospinal fluid (CSF). The Type B1 cells (dark blue) are radial glia-like quiescent NSCs which protrude a single primary cilium. They are in the center of a pinwheel structure formed by ependymal cells and extend an end-foot contact to blood vessels (Bv). The Type B2 cells (dark blue) are also radial glia-like NSCs but are proliferative and do not extent a primary cilium. The Type C cells (Green) are proliferative neural progenitors (TAPs), which are close to type B cells and also proximal to blood vessels. Type A cells (red) are neuroblasts and migrate along the rostral migratory stream (RMS) to the olfactory bulb. (Cartoon adapted from Ihrie and Avarez-Buylla, 2011 with modification)

Besides the morphological differences, the various cell types in the niche also express different markers. As summarized in Figure 1.3, the radial glia-like (with a cell body contacts the ventricles and a long radial process extending to the pial surface of the brain) quiescent NSCs (qNSCs) are both Prominin-1 (CD133) and Glial fibrillary acidic protein (Gfap) positive (Codega, et.al, 2014). Activated NSCs (aNSCs) express in addition the epidermal growth factor receptor (Egfr) at the cell membrane (Carrillo-Garcia et al., 2010; Obernier et al., 2011). whereas TAPs lack the expression of both Prominin-1 and Gfap but are still Egfr immunopositive when they differentiate into neuroblasts they lose their Egfr identity

(Carrillo-Garcia et al., 2010). Besides in NSCs, Gfap is also expressed in niche astrocytes and in a population of radial glia-like qNSCs, which lack the expression of Prominin-1 (Fischer et al., 2011; Codega et.al, 2014). Nestin is specifically expressed in neuro-epithelial stem cells (Lendahl et al., 1990) and is widely used as an NSC marker in mouse brain (Imayoshi et al., 2011). Many groups are using the Nestin-GFP or Gfap-GFP transgenic mice to mark the NSCs in the brain. However, different transgenic lines could yield different results because of the different genetic background caused by variable insertion site of the reporter gene (Fischer et al., 2011). Our group has developed a Fluorescence Activated Cells Sorting (FACS) approach to separate NSCs and their progeny without using transgenic lines. However, because of the lack of unique markers, NSCs and their progeny can be distinguished only by co-detection of multiple markers. For example, taking advantage of the two cell surface marker Prominin-1 (P) and Egfr (E), we could separately isolate qNSCs (P+E^{low}), aNSCs (P+E^{high}), TAPs (P-E^{high}) and neuroblasts (P-E^{low}) from the neonatal and adult SVZ (Carrillo-Garcia et al., 2010; Obernier et al., 2011; Khatri et al., 2014).

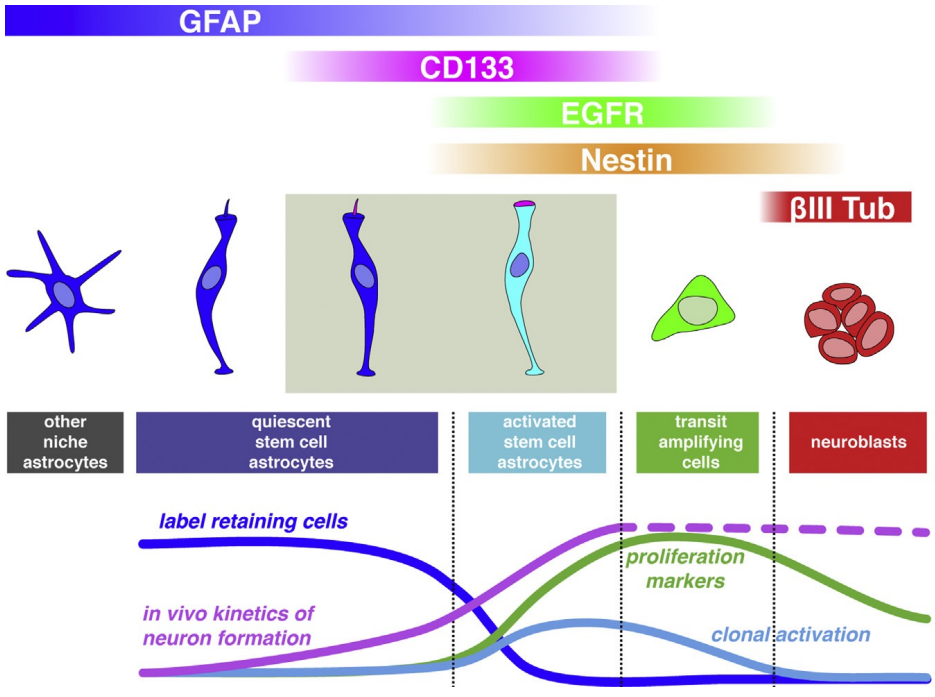

Figure 1.3 The cellular markers for SVZ stem cells and their progeny. Quiescent NSCs are Prominin-1 (CD133) positive and express Egfr at low levels. Activated NSCs are Prominin-1 positive and highly Egfr positive. TAPs are negative for Prominin-1 but still high express Egfr. Neuroblasts are Prominin-1 and Egfr negative. Of note, a subset of quiescent NSCs are also Prominin-1 negative but Gfap positive and to be distinguished from niche astrocytes through absence of extended processes. (Cartoon adapted from Codega et al., 2014)

1.3 The orphan nuclear receptor TLX and neurogenesis

Tlx (Tailless, NR2E1) was first identified in a screening of drosophila development mutants (Pignoni et al., 1990). The Tailless (*tll*) drosophila mutant has abnormalities in the terminal abdominal segment as well as in part of head structures and brain. The mouse *Tlx* gene was cloned by Monaghan et al., using the drosophila *tll* gene as template. The drosophila *tll* gene and its mouse homologue gene *Tlx* both code for a conserved orphan nuclear receptor specifically expressed in the eye and in the forebrain. During development of the mouse central nervous system (CNS) the TLX protein is detectable in the telencephalon, diencephalon, retina and olfactory placode (Yu et al., 1994; Monaghan et al., 1995). The expression of *Tlx* begins at embryonic day 8 (E8), peaks at E12.5, and then decreases from E13.5 until birth (Monaghan et al., 1995). After birth *Tlx* expression increases again to reach high expression levels in the adult brains. $Tlx^{-/-}$ mice appear normal at birth (Monaghan, et al., 1997). However, compared to the WT counterparts, adult mutant mice have severely reduced hippocampal dentate gyri, greatly expanded lateral ventricles and declined olfactory bulbs, indicating an impairment of neurogenesis (Monaghan et al., 1997; Shi et al., 2004) (Figure 1.4a). Moreover, $Tlx^{-/-}$ mice are more aggressive especially in males and therefore difficult to breed and handle. Taking advantage of a beta-galactosidase (beta-gal) reporter under the control of *Tlx* promoter, Shi et al. examined the expression pattern of *Tlx* in adult brains of heterozygote mice (Figure 1.4b). The reporter was found at high and dispersed pattern in the subgranular layer of the hippocampus DG as well as in a clustered pattern in the SVZ (Shi et al., 2004). All together, the highly enriched expression in the wild-type (WT) brain and the histological defects and behavior disorders of the $Tlx^{-/-}$ mice suggest that TLX plays an important role in neurogenesis and function of the brain.

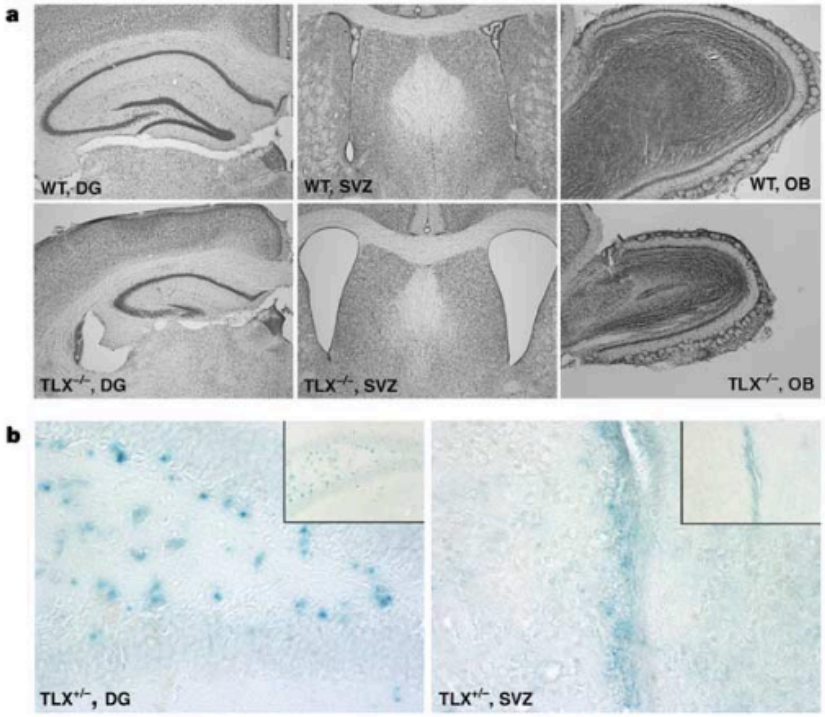

Figure 1.4 The Tlx expression pattern in the mouse SVZ. The histological observation of adult brains sections of both WT and *Tlx*$^{-/-}$ mice by Nissl staining (a). The beta-galactosidase (b-gal) reporter gene under control of the *Tlx* promoter was knocked in into the *Tlx* locus of *Tlx*$^{-/-}$ mice. The Tlx expression pattern (b) was shown in DG and SVZ of the adult heterozygouse *Tlx*$^{+/-}$ brain by LacZ staining (blue dots). (Figure adapted from Shi et al., 2004) Abbreviations: DG, dentate gyri; SVZ, subventricular zone; OB, olfactory bulb.

By using a TLX-specific antibody, Li et al. showed that TLX is expressed in both qNSC and TAPs in the SVZ of adult mouse brains (Li et al., 2012), which was consistent with our previous analysis of *Tlx* mRNA expression (Obernier et al., 2011). Loss of *Tlx* leads to a dramatic decrease in proliferation as shown by reduced BrdU incorporation and retention after pulse chase (Li et al., 2012). In fact, we found that, compared to the WT counterpart, activated aNSCs and TAPs are both reduced whereas the percentage of qNSCs increases in the *Tlx*$^{-/-}$ niche. Together these both findings underscored that TLX plays a key role in the regulation of NSC activation.

TLX mostly acts as a transcriptional repressor recruiting histone deacetylases (HDAC3 and HDAC5) to the promoters of its target genes, such as *p21* and *Pten* (Sun et al., 2007). However, TLX also activates the transcription of target genes such as the proneural factor *Mash1* by directly binding at its *Sp1* consensus sequence (Elmi et al., 2010). Moreover, TLX

has been shown to regulate neurogenesis through coordination of several signaling pathways according to the RNA-seq data (Niu et al., 2011). TLX activates Wnt7a/Beta-catenin signaling to stimulate NSC proliferation and self-renewal (Qu et al., 2009). In addition, *Tlx* can also be regulated by several mechanisms. For example, it was shown that MicroRNA-9 and MicroRNA-137 form a regulatory loop with Tlx and regulate the balance of NSC proliferation and differentiation (Zhao et al., 2009; Sun et al., 2011). MicroRNA let-7b and let-7d could also negatively regulate Tlx expression by targeting its 3'UTR (3' Untranslated region) (Zhao et al., 2010; Zhao et al., 2013). Interleukin-1β (IL-1b), which is the most predominant pro-inflammatory cytokine in the brain, could also negatively regulate *Tlx* expression (Ryan et al., 2013). All these data suggest that *Tlx* coordinates NSC proliferation and differentiation.

1.4 Notch signaling in the neurogenesis of the adult brain

The canonical Notch signaling is dependent on cell-cell contact and its activation needs the binding of a ligand from a donor cell to the Notch receptor of a signal-receiving cell (Figure 1.5) (Ables et al., 2011). Upon binding its ligand and proteolytic cleavage by the γ-secretase, the intracellular domain of Notch (NICD) is translocated into the nucleus where it interacts with the DNA-binding protein CSL (CBF1/RBPjκ/Su(H)/Lag-1) (Kopan et al., 2009; Ables et al., 2011). In the absence of NICD, CSL is associated with ubiquitous corepressor (Co-R) proteins and histone deacetylases (HDACs) to repress transcription of target genes. Upon NICD binding, transcriptional repressors are replaced by transcriptional coactivator Mastermind (MAM) and the transcription of downstream genes are activated. In mammals there are four different Notch receptors (Notch1, Notch2, Notch3, Notch4). And the five ligands are the Delta-like (Dll1, 3, 4) and Jagged (Jag1, 2) proteins. The typical Notch target genes are members of the Hes (such as Hes1 and Hes5) and Hey families. These target genes encode inhibitory basic helix-loop-helix (bHLH) proteins, which heterodimerize with bHLH activators such as NGN2 and MASH1 thereby inhibiting neuronal differentiation. As a feedback mechanism, proneural genes Ngn2 and Mash1 could also induce Delta expression, thereby activating Notch signaling and inhibiting neuronal differentiation of neighbor receiving cells (Kageyama et al., 2007).

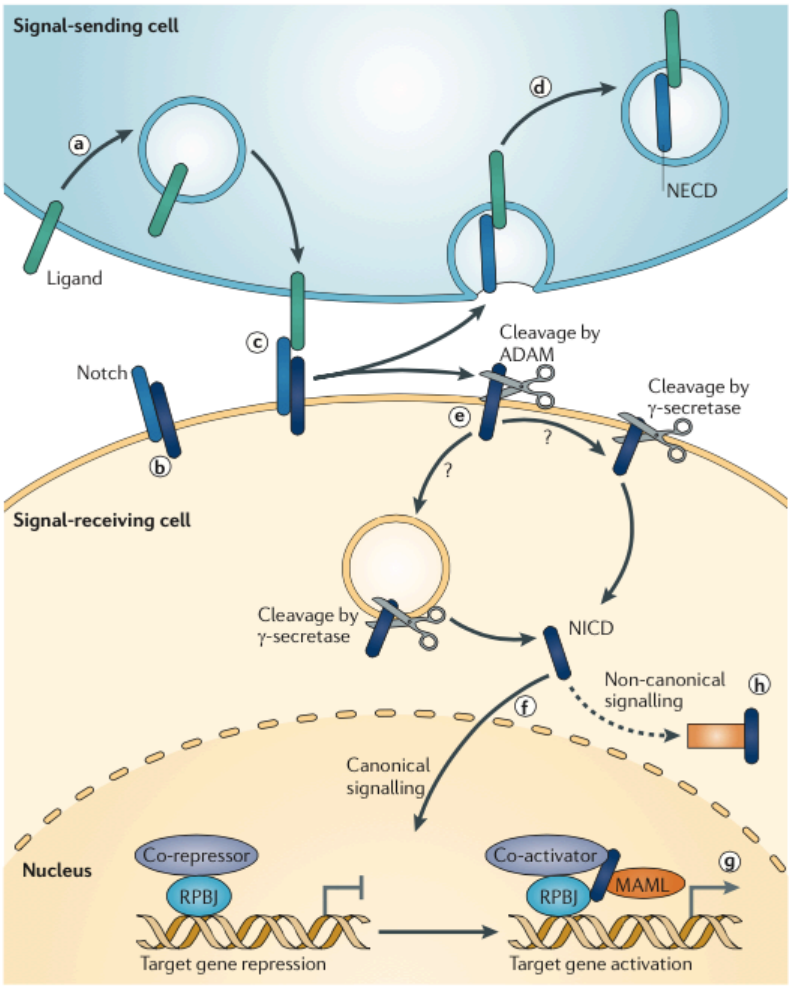

Figure 1.5 Schematic of canonical Notch signaling. The transduction of Notch signaling is based on the cell-cell interaction, which includes a 'signal-sending cell' that presents the Notch ligand and a 'signal-receiving cell', which expresses the Notch receptor. The activation of Notch signaling is triggered by the interaction of the ligand to the receptor. Upon activation, the Notch receptor is cleaved by γ-secretase and the Notch intracellular domain (NICD) is released and translocated into the nucleus. Thereafter, NICD replace the repressor complex on recombining binding protein suppressor of hairless (RBPJ or CSL) with a co-activator and initiate transcription of Notch target genes. (Cartoon adapted from Ables et al., 2011)

Because they are key effectors of the canonical Notch signaling, members of the Hes genes family have been intensively investigated in mutant mice. Knockout of *Hes1* and *Hes5* caused a premature neuronal differentiation and the severity of the phenotype was enhanced in *Hes1/Hes5* double knockout mice indicating the functional redundancy of these two genes (Ohtsuka et al., 1999). As a consequence of a negative feedback, *Hes1* is expressed in an oscillatory fashion with two hours periodicity, what may indicate that it regulates the timing of many biological processes (Hirata et al., 2002). However, *Hes1* is constitutively expressed in

boundary cells, which are not proliferating. In accordance to that, the proliferation of telencephalic neural progenitor cells is reduced when *Hes1* is overexpressed (Baek et al., 2006), indicating that *Hes1* may have an important role for regulating the cell cycle exit or maintenance of quiescence.

Normal brain development requires proper timing of differentiation programs. The Notch signaling is a key pathway in this regulation as it can modulate NSCs and neural development both spatially and temporally (Ables et al., 2011; Koch et al., 2013). Moreover, the components of Notch signaling are expressed throughout the adult brain, which suggests that Notch plays a role also in brain function (Berezovska et al., 1998). Notch regulates the cell cycle in order to control the balance of NSC maintenance and differentiation. The progenitors can be driven into quiescence by Notch induction, whereas the NSC division reinitiates upon blocking Notch (Chapouton et al., 2010). Knockout of Notch signaling components can deplete the NSC pool and increase the early progenitor cells. More intriguingly, the relative levels of Notch activity in NSCs can regulate the opposing states of quiescence versus proliferation. Low level of NICD leads to proliferation and high level causes growth arrest (Guentchev et al., 2006). However, the neuronal committed progenitors are less dependent on Notch and more responsive to environmental cues for the regulation of proliferation, suggesting that the capacity of Notch to regulate proliferation in the adult brain is cell type or cellular context dependent (Albes et al., 2010). As another layer of complexity, many of the Notch receptors have redundant roles, such as Notch3 may partially compensate the function of Notch1 receptor knockout mice (Mason et al., 2005). Furthermore, it has been recently determined that Notch signaling can be activated without ligands or the interaction with CSL which referred to as ‘non-canonical’ signaling (Andersen et.al, 2012). Therefore, neurogenesis is more intricately regulated by Notch signaling.

1.5 The aim of the work

The neurogenesis in the adult mammalian brain provides an important source of neurons for cell replacement therapies of the damaged brain. Although most of the adult NSCs are relatively quiescent, the investigation of the molecular mechanisms underlying their activation

would greatly benefit the clinical application. Previous research in our lab has found that *Tlx* is highly expressed in proliferative activated NSCs and TAPs and revealed a concomitant increase of Notch signaling target gene *Hes1* in activated NSCs (Obernier et al., 2011). Since neurogenesis is impaired in *Tlx* knockout ($Tlx^{-/-}$) mice, this model is suitable to investigate the mechanisms of NSC activation.

To understand the molecular mechanisms underlying the effect of TLX on NSC activation, my thesis will focus on:

1) Gene expression profile analysis of Notch signalling genes in NSCs isolated from age matched wild-type (WT) and *Tlx* knock-out/LacZ knock-in mice ($Tlx^{-/-}$).

2) Pharmacological inhibition of Notch signalling and loss of function approaches of *Hes1* on NSC activation in both WT and $Tlx^{-/-}$ mice.

3) Molecular biological analysis of TLX and *Hes1* interaction by reporter assays and chromatin immunoprecipitation (ChIP) to investigate whether TLX modulates *Hes1* gene transcription.

2. Materials and methods

2.1. Materials

2.1.1. General reagents

Reagents	Company
NP-40	CN Biomedicals Inco.
Ammonium chloride	Merck
Glycine	Life Technologies
Paraformaldehyde	Fluka
Isopropanol	Applichem
Mowiol	Calbiotech
Low Melting Agarose	Life Technologies
Ethanol	Sigma
Fetal bovine serum	Gibco
DPBS	Life Technologies

Equipments	Company
FACS	BD Aria II
Centrifuge	Eppendorf
4D Nucleofector System	Lonza
Real-time PCR System	ABI 7300
Microplate Luminometer	GloMax 96
Spectrophotometer	Pharmacia Biotech Ultraspec 300
Confocal Microscopy	Leica SP2

2.1.2. Plasmids

pFUGW (Lois et al., 2002)

pFUGW-Tlx(Constructed by Kirsten Obernier)

pLentilox3.7(Rubinson et al., 2003)

EF.mHES1.Ubc.GFP(Yu et al., 2006)

pCAGGS-NICD1(Dang et al., 2006)

pHes1(467)-luc (Nishimura et al., 1998)

pHes1-RBPJ(-)-Luc (Nishimura et al., 1998)

pHes5-Luc (Nishimura et al., 1998)

pRBPJ-AdTATA-Luc or p10XCBF1-luc (Mckenzie et al., 2006)

pAdTATA-Luc (Mckenzie et al., 2006)

pGL4.83[hRlucP/Puro]-EF1a-hRlucP (From Priit Pruunsild of Bading Group, IZN-Neurobiology, University of Heidelberg)

Lentivirus second generation packaging system plasmids:

pCMVdelta8.9 (Packaging plasmid) (Zufferey et al., 1997)

pVSVG (Envelope plasmid) (Naldini et al., 1996)

Lentivirus third generation packaging system plasmids:

(Dull et al., 1998)

pMDlg/pRRE (Packaging plasmid)

pRSV-Rev (Packaging plasmid)

pMD2.G (Envelope plasmid)

Adeno-associated virus (AAV) 2/1 packaging system plasmids:

pFdelta6

pRVI

pH21 (Hauck et al., 2003)

2.1.3. Reagents for DNA cloning

2.1.3.1 Primers and oligonucleotides

1. Sub-cloning primers of LentiLox3.7-Hes1-shRNA

Underlined letters are shRNA sequence specific for Hes1 mRNA, the *Italic letters* are restriction endonuclease recognization sequence and the **bold letters** are backbone to form stem and loop of shRNA. [shRNA sequence from (Kobayashi et al., 2009)]

1) Hes1-KD1 shRNA

Forward primer

5' *AAC* **G** GCCAATTTGCCTTTCTCATCC **TTCAAGAGA** GGATGAGAAAGGCAAATTGGC **CTTTTTT** *C* 3'

Reverse primer

5' *TCGAG* **AAAAAA**G GCCAATTTGCCTTTCTCATCC**TCTCTTGAA** GGATGAGAAAGGCAAATTGGC **C** *GTT* 3'

2) Hes1-KD2 shRNA

Forward primer

5' *AAC* **G** GTAGAGAGCTGTATTAAGTGA **TTCAAGAGA** TCACTTAATACAGCTCTCTAC **CTTTTTT** *C* 3'

Reverse primer

5' *TCGAG* **AAAAAA**G GTAGAGAGCTGTATTAAGTGA **TCTCTTGAA** TCACTTAATACAGCTCTCTAC **C** *GTT* 3'

2. Sub-cloning primers of pAAV-U6-Hes1-shRNA-CBA-GFP

1) Hes1-KD1 shRNA

Forward primer

5' *GATCC* **CC** GCCAATTTGCCTTTCTCATCC **TTCAAGAGA** GGATGAGAAAGGCAAATTGGC**TTTTTGGAA** *A* 3'

Reverse primer

5'*AGCTT* **TTCCAAAAA** GCCAATTTGCCTTTCTCATCC **TCTCTTGAA** GGATGAGAAAGGCAAATTGGC**GG** *G* 3'

2) Hes1-KD2 shRNA

Forward primer

5'*GATCC* **CC** GTAGAGAGCTGTATTAAGTGA **TTCAAGAGA** TCACTTAATACAGCTCTCTAC **TTTTTGGAA** *A* 3'

Reverse primer

5'*AGCTT* **TTCCAAAAA** GTAGAGAGCTGTATTAAGTGA **TCTCTTGAA** TCACTTAATACAGCTCTCTAC **GG** *G* 3'

3) Sequencing primer

Reverse sequencing primer (300bp downstream of the insertion site)

GAT GGG GAG AGT GAA GCA GA

4) WPRE sequence for quantify the AAV titration

Forward primer: ACTGTGTTTGCTGACGCAAC

Reverse primer: CAACACCACGGAATTGTCAG

5) Screening primers for the insertion of Hes1 shRNA into Lentilox3.7

Forward: CAGCACAAAAGGAAACTCAC

Reverse: GCGGTAATACGGTTATCCAC

Product: 238bp, with insertion: 320bp

2.1.3.2 Reagents and kits for DNA cloning

Reagents or Kits	Company
HpaI, XhoI, NheI.	NEB
Phusion High-Fidelity DNA Polymerase	NEB
T4 DNA ligase and ATP	Thermo Scientific
PureLink® HiPure Plasmid Filter Maxiprep Kit	Life Technologies
QIAquick® Gel Extraction Kit	QIAGEN
QIAquick® PCR Purification Kit	QIAGEN
QIAprep® Spin Miniprep Kit	QIAGEN

2.1.4 Reagents for cell culture and transfection and viral preparation

Reagents	Company
StemPro® Accutase Cell Dissociation Reagent	Life Technologies
Trypsin-0.05%EDTA	Gibco
EGF	Peprotech
huFGF2	Peprotech
B27 supplement	Gibco
DMEM, high glucose	Gibco
L-Glutamine 200 mM	Gibco
Penicillin/Streptomycin	Gibco
PI (propidium iodide)	Sigma
DNase I	Sigma
Ovomucoid	Sigma
Papain	Sigma

Euromed-N medium	Euroclone
Leibovitz's L-15 Medium	Gibco
Neurobasal-A Medium	Gibco
DAPT	Sigma
peqFECT DNA Transfection Reagent	peqlab
D-(+)-Glucose 45%	Sigma
Iscove's Modified Dulbecco's Medium(IMDM)	Life Technologies
Sodium Deoxycholate	Sigma
Benzonase	Sigma
HiTrap Heparin Column	Amersham
Amicon Ultra-4 Centrifugal Filter	Millipore

2.1.5 Antibodies

Primary Antibodies	**Company**	**Dilution**
Prominin-conjugated PE	Molecular probes	1:100-1:400
EGF-conjugated Alexa 647	Molecular probes	1:1000
Anti-NR2E1 Rabbit IgG	LifeSpan BioSciences, Inc.	1:100 for ChIP
Mash1 Mouse IgG	BD-Pharmingen	1:200
Ki67 Rabbit IgG	Abcam	1:500
NICD1 Rabbit IgG	Abcam	1:400
GFAP mouse IgG1	Sigma	1:1000

Secondary Antibodies	**Company**	**Dilution**
Mouse IgG-488	Mol.Probes	1:1000
Mouse IgG-cy3	Mol.Probes	1:500

Rabbit IgG-488	Mol.Probes	1:1000
Rabbit IgG-cy3	Mol.Probes	1:200
DAPI (1 mg/ml)	Sigma	1:1000

2.1.6 Reagents for RT-qPCR, luciferase assay and chromatin immunoprecipitation (ChIP)

Reagents or Kits	**Company**
TaqMan® Universal PCR Master Mix (2x)	Life Technologies
Arcturus® PicoPureRNA Isolation Kit	Life Technologies
RNeasy Micro or Mini Kit	Qiagen
Dual-Glo® Luciferase Assay System	Promega
Dynabeads® Protein G for Immunoprecipitation	Life Technologies
M-MLV Reverse Transcriptase	Promega
Oligo(dT) 15 primer	Promega
TaqMan® Universal PCR Master Mix	Life Technologies
Power SYBR® Green PCR Master Mix	Life Technologies

Probes for Taqman qRT-PCR

Actb	Mm00607939_s1
Ascl1 (Mash1)	Mm04207567_g1
Hes1	Mm01342805_m1
Notch3	Mm01345646_m1
Hes5	Mm00439311_g1
Notch1	Mm00435249_m1
Dll1	Mm01279269_m1

RBPj	Mm03053645_s1

2.1.7 Animals and cell lines

Both neonatal (p7) and adult (8 weeks) of WT and *Tlx*$^{-/-}$ mice are C57BL/6 genetic background. HEK293FT: established from human embryonic kidney cells transformed with the SV40 large T antigen (Life Technologies).

2.2 Methods

2.2.1 DNA cloning

2.2.1.1 Sub-cloning of LentiLox3.7-Hes1-shRNA

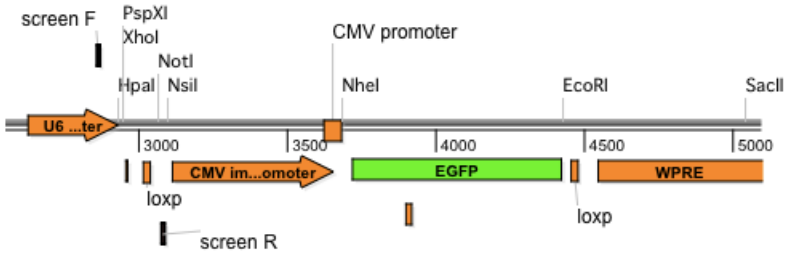

Figure 2.1 Schematic overview of LentiLox3.7 backbone for sub-cloning of Hes1 shRNA.

The Hes1 shRNA was cloned into the LentiLox3.7 by two restriction sites HpaI and XhoI which is under the control of U6 promoter. The EGFP (enhanced Green Fluorescent Protein) is driven by CMV promoter and followed by Woodchuck Hepatitis Virus posttranscriptional Regulatory Element (WPRE). The primers for amplifying the insert are also indicated as screen F and screen R.

1. Oligonucleotide designing strategy

1) Restriction enzyme sites

Two restriction enzyme sites were included in the oligonucleotide sequence of each shRNA according to the MIT protocol.

HpaI: GTT/AAC blunt end at 5'

XhoI: C/TCGAG sticky end at the 3'

2) Oligonucleotide format

Sense oligonucleotide: 5'AAC-(GN21)-(TTCAAGAGA)-(12NC)-TTTTTT-C3'

Antisense oligonucleotide: 5' TCGAG-AAAAAA-(GN21)-(TTCAAGAGA)-(12NC)- GTT 3'

The shRNA loop sequence (TTCAAGAGA) is based on the method of the paper Brummelkamp et al., Science, 2002.The two oligonucleotides were ordered through Eurofins with salt free purification.

2. Protocol (modified from the original MIT protocol)

1) The primers were annealed to obtain double strand shRNA with XhoI and HpaI restriction nuclease sites.

2) The LentiLox3.7 vector was cut with XhoI and HpaI and the digested fragments were separated by gel electrophoresis. Then the desired bands were purified with the Gel Extraction Kit.

3) The LentiLox3.7 backbone and Hes1-shRNA were ligated together with T4 ligase.

4) The ligation product was transformed into stlb3 competent *E. coli* and cultured with ampicillin selection at 37^{o}C.

5) Around 10 colonies were picked up and incubated at 37^{o}C for 2 hours and then the insertion of shRNA was checked by PCR.

6) The insertion of shRNA was confirmed by HpaI and NotI double restriction enzymes digestion. And there was a band shift of 70bp of positive cloning by 2% agrose gel compared to the lentiLox3.7 vector.

7) The shRNA insertion was sequenced by primer corresponding to FLAP (cagtgcaggggaa agaatagtagac) and the sequencing was conducted by GATC Biotech.

3. Solutions in the protocol

1). Annealing solution	**50 µl Total**
Sense Oligo (60 µM)	1 µl
Antisense Oligo (60 µm)	1 µl
ddH_2O	48 µl

The solution was incubated at 95°C 4 min, 70°C 10 min, cooled down at RT and stored at 4°C.

2). Restriction digestion	**20 ul Total**
pLentilox3.7	2 µg
10XBuffer	2 µl
XhoI	1 µl
HpaI	1 µl
ddH_2O	Add to 20 µl in total

The digestion was conducted at 37°C water bath for 1-2 h and stopped by incubating it at 65°C for 10 min.

3). Ligation	**10 µl total**
pLentiLox3.7 backbone	60 fmol
Annealed oligo	60 fmol
T4 Ligase	1 µl
10X T4 Ligase buffer	1 µl
ATP (100 mM)	0.5 µl
ddH_2O	Add to 10 µl in total

The backbone and the oligonucleotides were ligated at RT for 1 h and the ligation was stopped by incubating at 65°C for 10 min.

2.2.1.2 Sub-cloning of pAAV-U6-Hes1-shRNA-CBA-GFP

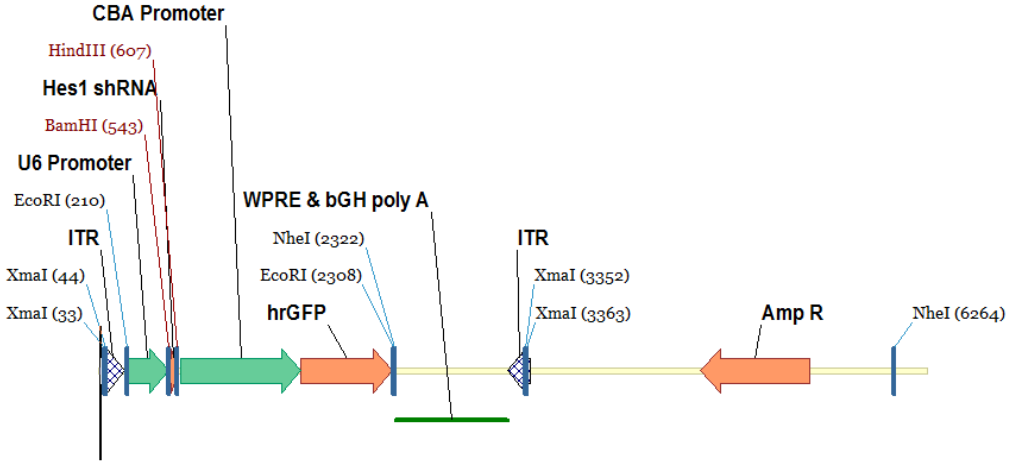

Figure 2.2 Schematic overview of pAAV-U6-CBA-GFP backbone for sub-cloning of Hes1 shRNA.

The Hes1 shRNA was cloned into the pAAV-U6-CBA-GFP by two restriction sites BamHI and HindIII which is under the control of U6 promoter. The hrGFP (humanized recombinant Green Fluorescent Protein) is driven by CBA (chicken beta-actin) promoter and followed by Woodchuck Hepatitis Virus posttranscriptional Regulatory Element (WPRE) and bGH (bovine growth hormone) polyA signal.

1) Restriction enzyme sites

Two restriction enzyme sites are included when synthesize the oligos of shRNA

BamHI: G/GATCC at 5' end

HindIII: A/AGCTT at 3' end

2) Oligonucleotide format

Sense oligonucleotide: 5'GATCC-CC-(GN21)-(TTCAAGAGA)-(12NC)-TTTTTGGAA-A3'

Antisense oligonucleotide: 5' AGCTT-TTCCAAAAA-(GN21)-(TTCAAGAGA)-(12NC)- GG-G 3'

The protocol is same as the subcloning of pLentilox-3.7-Hes1-shRNA just with two different restriction enzymes BamHI and HindIII. And the sequencing primer is a reverse primer located in the WPRE element (GAT GGG GAG AGT GAA GCA GA).

2.2.2 Cell culture and virus production

2.2.2.1 HEK293FT cell culture

The HEK293FT cells were used for producing lentivirus or adeno-associated virus. The cells were cultured in 10 cm tissue culture dishes with DMEM complete medium. The cells were

passaged every 2-3 days with a splitting ratio of 1:4. During passage, the culturing medium was removed and the cells were gently washed twice with 0.1 M phosphate buffered saline (PBS). And 0.5 ml Trypsin-EDTA (0.05%) was added directly onto the cells after removing PBS, and the dish was incubated at 37^{o}C for 1 min. And then, 2 ml DMEM-complete medium was added into the dish to stop the enzyme digestion. Cells were dissociated into single-cell suspension by pipetting 3-5 times and collected in a 15 ml falcon tube. The cell suspension was spun down at 800 g for 2 min to remove the supernatant. The cells were aliquoted into new dishes with prewarmed DMEM complete medium.

DMEM complete medium	
DMEM, high glucose (4.5g/L)	500 ml
Heat-inactivated FBS[#]	50 ml
Pen/Strep	2.5 ml

[#] FBS was inactivated at 56^{o}C for 30 min.

2.2.2.2 Lentivirus production and purification

2.2.2.2.1 Lentivirus production

1. The 3X10^{6} HEK293FT cells were pre-seeded in a 10 cm dish the previous day in order to get 80% confluence before transfection; 4X10 cm dishes were prepared for each virus.

2.The following plasmids were mixed in 450 µl ddH_2O in a 15 ml tube.

For each 10 cm dish

pHCMVG	6 µg
pMDLg/pRRE	10 µg
pRSV-Rev	5 µg
Virus plasmid	20 µg

3. The 50 µl 2.5 M $CaCl_2$ was added into the mixture prepared last step and mixed well.

4. Then 500 µl 2XHeBS was added dropwise to the mixture while shaking the tube to thoroughly mix the two solutions.

5. The solution was incubated at RT for 30 min before being added onto the cells.

6. After 6 hours the supernatant was replaced with fresh medium. Thereafter, the supernatant was collected at the time point of 48 h and 72 h after transfection and stored at 4^{o}C before purification.

2XHeBS	
HEPES	50 mM
NaCl	280 mM
Na_2HPO_4	1.5 mM

2.2.2.2.2 Lentivirus purification by Abm speedy lentivirus purification kit

1. The viral supernatant was spun at 2500 g for 10 min and filtered through a 0.45 μm PVDF syringe filter to get rid of cell debris.

2. Then 5 ml lenti-binding solution was added into 45 ml viral supernatant and mixed completely by turning upside down the tube several times.

3. The mixture was centrifuged at 5000 g for 30min at 4^{o}C and then the supernatant carefully disposed without disturbing the pellet.

4. The viral pellet was resuspended in 3.5 ml DPBS solution and loaded into an Amicon Ultr-4 centrifugal filter unit.

5. The loaded filter unit was centrifuged at 5000 g for 10min and washed twice with DPBS. And the virus was reconstituted in 100-300 μl DPBS. The virus was aliquoted into 20 μl each tube and stored at -80^{o}C.

2.2.2.2.3 Titering of lentivirus

1. The 3X10^{4} HEK293FT cells were seeded in each well of a 96-well plate 24 hours before titration.

2. The original viral stock was diluted up to 10^{6} times by serial 10-fold dilutions.

3. The infected cells were cultivated at 37^{o}C for 48 h to express the GFP tag.

4. The GFP positive cells were counted under the fluorescence microscope and the titration was calculated by the formula below:

Titer (TU/mL)= GFP+ cell number/virus volume.

5. The titer could also be measured by using FACS to analyze the percentage of GFP+ cells.

Titer (TU/mL)= (GFP+ cell) % X total seeded cell Number/virus volume.

2.2.2.3 Adeno-associated virus production and purification

2.2.2.3.1 Adeno-associated virus production

For each AAV virus, the HEK293 cells in 5X14 cm dishes were transfected.

1. The medium in 14 cm dishes was replaced with 25 ml pre-warmed IMDM 2 h before transfection.

2. The transfection mixture was prepared by adding ingredients into a 15 ml tube in the following order: ddH_2O, $CaCl_2$, plasmids:

ddH_2O	12 ml
2.5 M $CaCl_2$	1.65 ml
AAV plasmid	62.5 µg
pFdelta6	125 µg
pRVI	31.25 µg
pH21	31.25 µg

3. After preparing the mixture, 13 ml 2XHeBS was added dropwise while shaking the tube to thoroughly mix the two solutions.

4. The transfection solution was added dropwise onto the cells and mixed by swirling gently.

5. The cells were incubated at 37^{o}C. After six hours the medium was replaced with DMEM complete medium and plates were returned to the incubator for further 60 hours.

2.2.2.3.2 AAV purification

1. Harvest the cells 60-65 h later

1) The cells were washed gently with 0.1 M PBS twice and detached by cell scraper.

2) The cells were centrifuged at 800 g for 5 min to obtain the cell pellet.

3) The pellets were pooled together from 5X14 cm dishes and resuspended in 50 ml 150 mM NaCl/20 mM Tris solution.

4) Thereafter the cell suspension was aliquoted into two 25 ml lots in 50ml tube and frozen at -20^{o}C overnight.

2. Benzonase treatment to remove cellular DNA and RNA

1) The fresh 10% sodium deoxycholate solution was prepared in H_2O.

2) Then 1.25 ml 10% sodium deoxycholate was added to each 25 ml cell suspension (for a final concentration of 0.5%) along with 5.10 ml 250 U/ml benzonase (for a final concentration of 50 U/ml).

3) The solutions were mixed completely and incubated in a 37°C water bath for 1 h.

4) The mixture was centrifuged at 3000 g for 15 min at 4°C and the supernatant was transferred into a new tube. (Stored at –20°C until column purification)

3. Heparin column purification

1) The heparin column was pre-equilibrated with 10 ml 150 ml NaCl/20 mM Tris solution at a flow rate of 1 ml/min.

2) The 50 ml virus supernatant was loaded into a 60 ml syringe and washed through the column at a flow rate of 1 ml/min.

3) Then the column was washed with 20 ml 100 mM NaCl/20 mM Tris at a flow rate of 1 ml/min by using a 60ml syringe.

4) The column was washed with 1 ml 200 mM NaCl/20 mM Tris and 1 ml 300 mM NaCl / 20 mM Tris solutions, respectively.

5) The virus then was eluted into a sterile 15 ml tube with1.5 ml 400 mM NaCl/20 mM Tris, 3.0 ml 450 mM NaCl/20 mM Tris and 1.5 ml 500 mM NaCl/20 mM Tris solutions respectively.

6) The virus was concentrated with Amicon Ultra-4 filter by centrifuging at 2000g for 3 min followed by washing with 3.5 ml DPBS twice.

7) The virus was concentrated on the filter (around 250 ul). The concentrated virus then was filtered through a 13 mm, 0.2 µm syringe filter and stored at -20^{o}C.

2.2.2.3.3 AAV genomic tittering

1. Extraction of viral DNA

1) The viral stock was digested by DNase I to remove non-viral DNA by incubating at 37°C for 30 min

Virus	2 µl
10X DNase buffer	10 µl
DNase I (Life Technologies)	1 µl
ddH_2O	86 µl

2). The Dnase I activity was stopped by incubating the solution at 70°C for 10 min followed by adding 1µl proteinase K and incubating at 50°C for 1 h to remove the viral capsid and protein.

3). The Proteinase K was inactivated by incubating at 95°C for 20 min and the viral DNA was stored at 4°C before genomic tittering.

2. Genomic titration

1). A serial of dilutions of a reference plasmid were prepared at 10^{10},10^{9},10^{8},10^{7}, 10^{6}, 10^{5}, and 10^{4} copies/ml for standard curve and ddH_2O was included for non-template control.

2). A master mix was prepared as below and the tittering was analyzed with qPCR

Master Mix	**20 µl total**
Sense primer (10µM)	0.4 µl
Antisense primer (10µM)	0.4 µl
Sybr Green Mix (2X)	10 µl
ddH2O	8.2 µl
Viral DNA or Reference plasmid	1 µl

3). The titre was calculated by multiplying the qPCR production concentration with 10^{5} for viral particles per ml.

2.2.3 SVZ dissection and FACS

1. NSA complete	**Total 10 ml**
NS-A medium	9.8 ml
L-Glutamine 200 mM	100 µl
Pen/Strep	100 µl
2. E/F Medium	**Total 10 ml**
NSA Complete	10 ml
B27 Supplement	200 µl
huFGF-2 (Stock 20 µg/ml)	5 µl (Final 10 ng/ml)
huEGF recom (Stock 20 µg/ml)	10 µl (Final 20 ng/ml)
3. Sort medium	**Total 10 ml**
NSA complete	5 ml
Leibowitz L15 Medium	5 ml
B27 supplement	200 µl
FBS	100 µl
D-(+)-Glucose 45%	133 µl
huFGF-2 (Stock 20 µg/ml)	5 µl
DNAse (Stock 0.1% in ddH_2O)	100 µl
4. NBA collecting medium	**Total 10 ml**
Neural Basal A medium	9.8 ml
L-Glutamine 200 mM	100 µl
Pen/Strep	100 µl
B27 supplement	200 µl
huFGF-2 (Stock 20 µg/ml)	5 µl

5. Dissection solution (pH 6.9)	Dissolved in ddH_2O and filter to sterile
150 mM	Sucrose
125 mM	NaCl
3.5 mM	KCl
1.2 mM	NaH_2PO_4
2.4 mM	$CaCl_2 \cdot 2H_2O$
1.3 mM	$MgCl_2 \cdot 6H_2O$
0.1%(6.65 mM)	Glucose
2 mM	Hepes
6. Papain stock solution 2X	Dissolved in 60 ml 0.1 M PBS and filter to Sterile
Papain	100 mg
L-Cystein	20 mg
EDTA	20 mg
7. Ovomucoid stock solution 2X	Prepared in 0.1 M PBS and filter to Sterile
Trypsin Inhibitor	1.4 mg/ml

2.2.3.1 SVZ dissection and dissociation

SVZ tissues were obtained from the brain of postnatal 7 days mice (p7) or 8 weeks old adults of Tlx line. P7 mice were killed by decapitation and the adults were killed by neck dislocation after the CO_2 anesthesia in accordance with the ethical guidelines for the care and use of laboratory animals (Karlsruhe, Germany). The SVZ was dissected in ice-cold sucrose dissection solution and dissociated into single cells firstly by papain digestion at 37^{o}C for 3 min. The digestion was stopped by equal volume of ice-cold Ovomucoid solution. Then the tissue was dissociated into single cells by pipetting 10 time with 1 ml tip and then 20 times with 200 µl tip in 400 µl sort medium. The cells were filtered through a 35 µm cell strainer cap of BD

Falcon tube. The dissociated cells can be used for neurosphere culture in E/F medium or stained for sorting.

2.2.3.2 Cell staining and FACS

The cells were stained both with Prominin-PE (1:100) and EGF-Alexa 647(1:1000) to get a four-population sort. The gates of different populations were set according to the controls list below:

Autofluorescence	Without any staining (For FSC or SSC setting)
Autofluorescence+ PI (Propidium iodide)	Stained only with PI (For PI gate setting)
Prominin Positive Control	Stained only with Prominin-PE (For Prominin positive gate setting)
Block Control	The cells were blocked with EGF before staining with EGF-Alexa647 (For EGF^{low} gate and EGF^{high} gate setting)
EGF Positive Control	Stained only with EGF-Alexa647 (to confirm the EGF^{high} gate setting)

The cells were sorted into 1.5 ml or 0.5 ml Eppendorf tubes after finishing the gate setting at a threshold of 300-500 events per second. For clonal analysis, the cells were sorted directly into a 96-well plate, which was pre-filled with warm medium.

2.2.4 RNA extraction and Taqman gene expression assay

2.2.4.1. RNA Extraction and retro-transcription into cDNA

The cells were sorted directly into RNA lysis buffer with a ratio of 10 µl per 1000 cells. And the cells were homogenized by brief vortexing for 30 s after sorting. RNA was extracted according to the protocol recommended by the manufacturer. Briefly, the lysate was mixed with one volume 70% ethanol before transferring into the spin column. Spin down to discard the flow-through. Wash the column with 700 µl RW1, 500 µl RPE and 500 µl 70% ethanol

respectively. The RNA was eluted with 14 µl RNase-free ddH_2O after discarding the residual washing buffer with a full speed of centrifuge. The RNA was retro-transcribed into cDNA directly after the extraction. 10 µl RNA was annealed with 2 µl OligodT(15) at 80^oC for 3 min. And the mixture was transcribed into cDNA with following protocol.

Total	**30 µl**
RNA	12 µl
5X M-MLV buffer	6 µl
dNTPs (10 mM)	1.5 µl
DTT (100 mM)	3 µl
M-MLV Reverse Transcriptase	2 µl
RNasin (40 U/µl)	0.7 µl
RNase-free ddH_2O	4.8 µl

All the reagents were mixed well and incubated at 42^oC for 60 min and then the reverse transcription was stopped by incubation at 80^oC for 10 min. The cDNA was diluted in 90 µl RNase-free ddH_2O and stored at -20^oC before qPCR.

2.2.4.2. Taqman gene expression assay

To analyze the mRNA expression of different populations of both WT and *Tlx*$^{-/-}$, the Taqman gene expression assay was used. The analysis was based on the pre-designed probes for the interested genes. And beta-actin was chosen as reference gene.

Taqman Assay Mixture	**20 µl total**
Taqman Master Mix (2X)	10 µl
Probe	1 µl
RNase-free ddH_2O	4.5 µl
cDNA	4.5 µl

The mixture was denatured at 95^{o}C for 10 min and followed by 50 cycles of 95^{o}C denature for 15 s and annealing at 60^{o}C for 1 min. And the data was collected during the annealing procedure.

2.2.5 Luciferase assay and chromatin immunoprecipitation assay (ChIP)

2.2.5.1. Luciferase assay

1. Luciferase assay with HEK293FT cells

Around 3-4X10^{4} cells each well of 96-well plate were seeded 24 h before transfection. The plasmids were prepared as listed below (with or without NICD) in 75 µl Opti-MEM for triplicate wells. 9 µl peqFECT DNA transfection reagent was added and mixed well. The mixture was incubated at RT for 20 min before aliquoting to three wells. The luminescence was measured 48 h after transfection according to the protocol of manufacturer. Briefly, 75 µl of Dual-Glo reagent was added into each well to lysate cells. The firefly luminescence was measured 10 min later in a luminometer. And then 75 µl Dual-Glo Stop & Glo reagent was added to quench the firefly luminescence and trigger the Renila luminescence. The Renila luminescence was measured 10 min later. The ratio of firefly to Renila luminescence was calculated for each well and then normalized the ratio to control (FUGW). All the experiments were done in triplicate and the samples were transferred into a 96 well plate with opaque walls before measuring luminescence.

Without NICD Cotransfection		**With NICD Cotransfection**	
FUGW or FUGW-Tlx	375 ng	FUGW or FUGW-Tlx	375 ng
Luciferase Reporter plasmid	375 ng	Luciferase Reporter plasmid	375 ng
Renila Reporter plasmid	7.5 ng	Renila Reporter plasmid	7.5 ng
		pCAGGS-mNICD1	375 ng

2. Luciferase assay in neurosphere cultures

The SVZ cells were derived from p7 WT pups and dissociated into single cells for neurosphere formation in E/F medium at a density of 10^5 cells/ml. Neurospheres were formed after 5-7 days culture in a 37°C humidified incubator with 5% CO_2. The neurospheres were dissociated into single cells after incubating with Accutase for 5 min at 37°C. The single cells were either expanded or transfected. $5X10^5$ single cells were transfected by 4D-Nucleofector with a 16 well nucleocuvette. The cells were spun down to remove medium and cells pellet was resuspended by 20 µl P3 primary cell solution contained the plasmids listed below. The cells were transferred into one well of the cuvette and pulsed with DS113 program and then respuspended with 180 µl prewarmed E/F medium for each well. The transfected cells from one nucleocuvette well were transferred into one well of 6-well plate for further culture of 48 h. The cells were collected and aliquoted into two wells of a 96 well plate with opaque walls to measure the luciferase assay. And the protocol is same as HEK cells shown above.

FUGW or FUGW-Tlx	2.5 µg
Luciferase Reporter plasmid	2.5 µg
Renila Reporter plasmid	50 ng
pCAGGS-mNICD1	2.5 µg

2.2.5.2 Chromatin immunoprecipitation assay (ChIP)

The neurospheres derived from adult WT SVZ were used for ChIP. The culture and the expansion of the neuroshperes were same as the neurospheres derived from p7 mice. $1X10^6$ single cells were used for transfection. 5 µg FUGW-Tlx along with 4 µg pCAGGS-NICD1 were transfected into cells by 4D Nucleofector. The cells were cultured in E/F medium for 48 h before fixed with formaldehyde. The protocol was modified from Magna ChiP A Kit (Millipore).

1. Reagents for the ChIP

Cell lysis buffer

Hepes pH 7.9	10 mM
$MgCl_2$	1.5 mM
KCl	10 mM
Igepal	0.5%

Nuclear lysis buffer

SDS	1%
EDTA	10 mM
Tris-HCl pH8.1	50 mM

Dilution buffer

SDS	0.01%
Triton-X100	1.1%
EDTA	1.2 mM
Tris-HCl pH8.1	16.7 mM
NaCl	167 mM

Low salt wash buffer

SDS	0.1%
Triton-X100	1%
EDTA	2 mM
Tris-HCl pH8.1	20 mM
NaCl	150 mM

High salt wash buffer

SDS	0.1%
Triton-X100	1%

EDTA	2 mM
Tris-HCl pH8.1	20 mM
NaCl	500 mM

LiCl wash buffer

LiCl	0.25 M
Igepal	1%
SOD	1%
EDTA	1 mM
Tris-HCl pH8.1	10 mM

TE buffer

Tris-HCl pH8.1	10 mM
EDTA	1 mM

ChIP elution buffer

SDS	1%
NaHCO3	50 mM
Tris-HCl pH8.1	50 mM
EDTA	1 mM
Proteinase K (add before use)	50 ng/µl

2. Primers for qPCR

Hes1 promoter specific primers

Sense 5’ CTGGGCTTTGCTTAGTTT 3’

Antisense 5’ TTTACCTTGTTCCCTCCT 3’

Hes5 promoter specific primers

Sense 5’GCACGCTAAATTGCCTGTGA 3’

Antisense 5’ CCCGGGATGCTAATGAGGAC3’

3. Crosslinking and lysis of the cells

The protein and DNA were crosslinked by adding 230 µl 37% formaldehyde (final concentration 1%) into 10 ml medium at RT for 10 min. The crosslink was stopped by adding 1 ml 1.25 M Glycine and incubating at RT for 5 min. The cells were collected by centrifuge at 800 g for 5 min at 4^{o}C. And the cell pellet was washed twice with 2 ml ice-cold PBS containing 20ul Protease Inhibitor Cocktail II (PIC) (Roche, 25X solution). The cell pellet was resuspended in 500 µl Cell Lysis buffer containing 5 µl PIC. The cell suspension was incubated on ice for 15 min and then vortexed every 5 min. Centrifuge to collect the pellet and resuspended in 200 µl Nuclear Lysis buffer containing 2 µl PIC. The DNA of cell suspension was sheared into 200-1000 bp in length by sonicating for 5 min with 30 s off in between 30 s pulses in ice water slurry bath. The debris was removed by centrifuge 15,000 g for 10 min at 4^{o}C. The supernatant was aliquoted into 50 µl and stored at -80^{o}C for up to three months.

4. Immuniprecipitatioin (IP) of cross-linked protein/DNA complex

Remove two 50 µl aliquots from -80^{o}C and diluted in 450 µl Dilution buffer (5 µl PIC). Take 1% solution as input. And add 5 µl Tlx rabbit IgG or 2 µl normal rabbit IgG into each aliquot and incubate at 4^{o}C for 1 h before adding 20 µl Protein G beads for overnight incubation. The next day wash the magnetic beads with 500 µl of each Low Salt Wash Buffer, High Salt Wash Buffer, LiCl Wash Buffer and TE Buffer for 3-5 min in 4^{o}C cold room, sequentially.

5. Elute the protein/DNA complex and free the DNA

The protein/DNA complex was eluted from the beads by incubating them with 100 µl Elution buffer which contains 1 µl proteinase K at 62^{o}C for 1 h on a shaking plate. Both the inputs and samples were treated with proteinase K. The proteinase K was inactivated at 95^{o}C for 10 min. The DNA was purified with Qiaquick PCR Purification Kit and resolved in 50 µl ddH_2O.

6. qPCR to analyze the enrichment of protein/DNA complex

Take 2 µl of either input or sample to the master mixture list below and analyze the enrichment by qPCR. The samples were denatured at 95^{o}C for 10 min and followed by 43 cycles of 10 s

95°C denature and 1 min 58°C annealing. The data was collected at annealing procedure. All the experiments were done in triplicate. The signal of the sample was calculated as $2^{-(Ct\ sample-Ct\ input)}$. The fold enrichment is expressed as the ratio of Tlx rabbit IgG signal to Normal rabbit IgG signal.

Total	**18 µl**
SYBR-Green Master Mix (2X)	10 µl
ddH_2O	7 µl
Primer mix (20 µM)	1 µl

2.2.6 Stereotactic injection and slicing

The mice were fixed in a stereotactic frame after the sedation with sleeping mix. The bregma was used to locate the ventricle. 1 µl DMSO or 10 mM DAPT was injected into the ventricle with the coordinates of AP 0 mm, ML 1 mm, DV 2 mm for WT and AP 0.5 mm, ML 0.5 mm, DV 2 mm for *Tlx*$^{-/-}$ mice. When the virus was injected, the coordinates of AP 1.2 mm, ML 0.5 mm and DV 2.5 mm were used for both WT and *Tlx*$^{-/-}$ mice. The liquid was applied with a pump-driven nanofil syringe (10µl) at a speed of 200 nl/min. The needle of the syringe was pulled out slowly 5 min after the completion of the injection. The mice were woken up with waking up mix along with painkiller after the skin was stitched up. The mice were placed on the 38-40°C heating plate during the surgery and the cages were kept on heating plate 24-48 h more to let the mice to recover.

Sleeping Mix	**7 ml total**
0.9% NaCl	4.5 ml
Dormitor (1 mg/ml Medetomedin)	0.5 ml
Dormicum (5 mg/ml Midazolam)	1 ml
Fentanyl (0.05 mg/ml)	1 ml

Waking Mix	**8.5 ml total**
Antisedan (5 mg/ml atipamezol)	0.5 ml
Anexate (0.1 mg/ml Flumazenil)	5 ml
Naloxon (0.4 mg/ml Naloxon)	3 ml
Painkiller	**5 ml total**
0.9% NaCl	4.75 ml
Temgesic (0.324 mg/ml Buprenorphin)	0.25 ml

2.2.7 Immunohistochemistry and immunocytochemistry

2.2.7.1 Immunohistochemistry

The mice brains were perfused with 10% formalin after i.p. injection of 50 µl sodium-pentobarbital (Narcoren, Merial, 400 mg/kg body weight). The brains were removed and fixed in 10% formalin 4^{o}C overnight. After washes with 0.1 M PBS, brains were embedded in 4% low melt agarose. Coronal sections were cut at a thickness of 40 µm with Vibratom and then processed for immunohistochemistry. The slices were permeabilized by NP40 for 30 min and the residual formalin was quenched by 0.1 M glycine/ 0.1 M PBS and 50 mM NH_4Cl/0.1M PBS for 30 min sequentially. And primary antibody was applied overnight at 4^{o}C after immersing the slices in 5% FCS/0.1 M PBS for 1 h at RT. The secondary antibody was applied for 1 h at RT after washing the slices three times with 0.1 M PBS. All the antibodies were diluted in 5% FCS/0.1M PBS. DAPI was used for nuclear counterstaining for 1 min at RT. The slices were mounted onto the glass slides with Mowiol after washing with ddH_2O and drying with filter paper. The Mowiol was dried at RT for 1-2 h and the slices were stored at 4^{o}C until taking image.

2.2.7.2 Immunocytochemistry

The sorted cells were incubated for extra 4 h in F medium to attach to the matrigel pre-coated chamber slide. Cells were fixed in 3% paraformaldehyde in PBS that contains 4% sucrose for 10-15 min, then rinsed twice with 10 mM glycine/0.1 M PBS. The cells were either stored at 4°C in 10 mM glycine/0.1M PBS or permeabilized in 0.5% NP-40/0.1 M PBS for 5 min. The primary antibodies were applied overnight at 4°C after rinsing the cells with 0.1 M PBS twice. The next day, the secondary antibody was applied to the cells for 1 h at RT after washing the cells three times with 0.1 M PBS. The cell nuclei were stained with DAPI. Around 5-10 µl of Mowiol was placed on each well of the chamber-slide and a 24 mm X 60 mm glass coverslip was gently placed on top of it. And air bubble should be avoided.

2.2.7.3 Confocal microscopy

All the images were acquired using a laser scanning confocal microscope (Leica TCS SP2). Three slices each mice were used for immunohistochemistry and imaging.

2.2.8 Statistics

All the imaging data were analyzed with LCS lite (Leica Confocal Software) and Image J. Statistic analysis was performed with two-tailed homoscedastic Student's T test or paired T test by SigmaStat (n.s.: not significant; *: $p < 0.05$; **: $p < 0.01$; ***: $p < 0.001$). Graphs were made with Microsoft Excel 2007 and Adobe illustrator CS4.

3. Results

3.1 Neurogenesis is impaired in *Tlx*$^{-/-}$ mice

3.1.1 Comparative analysis of the various precursor types in the WT and *Tlx*$^{-/-}$ SVZ

Neural stem cells (NSCs) in the adult mammalian brain continue to generate new neurons throughout the life span of the animal. Adult NSCs are relatively quiescent and undergo cell division only upon cell cycle entry. An essential regulator for promoting cell cycle entry of adult NSCs is the nuclear orphan receptor Tailless (*Tlx*) and mice lacking *Tlx* display reduced hippocampal dentate gyri, greatly expanded lateral ventricles and reduced olfactory bulbs, indicating a greatly impaired neurogenesis (Monaghan et al. 1997).

To investigate the molecular mechanisms underlying the impairment of neurogenesis in *Tlx*$^{-/-}$ mice, our group has developed a fluorescence activated cell sorting (FACS) based approach. By measuring the levels of Prominin-1 (P) and EGFR (E) expression at the surface of dissociated SVZ cells we were able to separate quiescent NSCs (qNSCs) in the P+E- population and activated NSCs (aNSCs) and their immediate progeny transit-amplifying precursors (TAPs) in the P+E+ and P-E+ subsets, respectively. We also found that the last population of P-E- cells represents mostly neuroblasts if the cells are isolated from the neonatal SVZ (Carrillo-Garcia et al., 2010; Cesetti et al., 2009). Instead when cells are isolated from the adult SVZ, this population includes a large fraction of niche astrocytes (Khatri et al., 2014). To establish correct gate setting I used various controls, including, an autofluorescence control was used to obtain the intact cell gate (P2 gate) to exclude cell debris and doublets (Figure 3.1 A). And the cells stained only with propidium iodide (PI) were used to set the viable cell gate (P3 gate) to exclude the dead cells during the sample preparation procedure (Figure 3.1 B). These controls were used also to establish the negative gate for Prominin-1 staining (Figure 3.1 D). In contrast, to determine EGFR expression I used an Alexa647-conjugated EGF (Ciccolini et al., 2005). Negative gates in this case were set based using cells pretreated with EGF before staining with EGF-Alexa647, to control for unspecific binding of EGF-Alexa647 on the cell surface (Figure 3.1 C). On average, the Prominin-1 immunopositive

cells represented were set based on WT control with an average yield of 1-2% of all cells which were selected as Prominin-1 positive (P+) (Figure 3.1 F) while the EGFR gate sorted only 1.5-2.5% $EGFR^{high}$ cells (E+) (Figure 3.1 E). The P+E-, P+E+, P-E+ and P-E- cells were sorted according to the intersectional gate settings of Prominin-PE and EGF-Alexa 647. Representative plots of these four populations in both WT (Figure 3.1 E, F, G, H) and KO (*Tlx*$^{-/-}$) (Figure 3.1 I, J, K, L) are shown below, respectively.

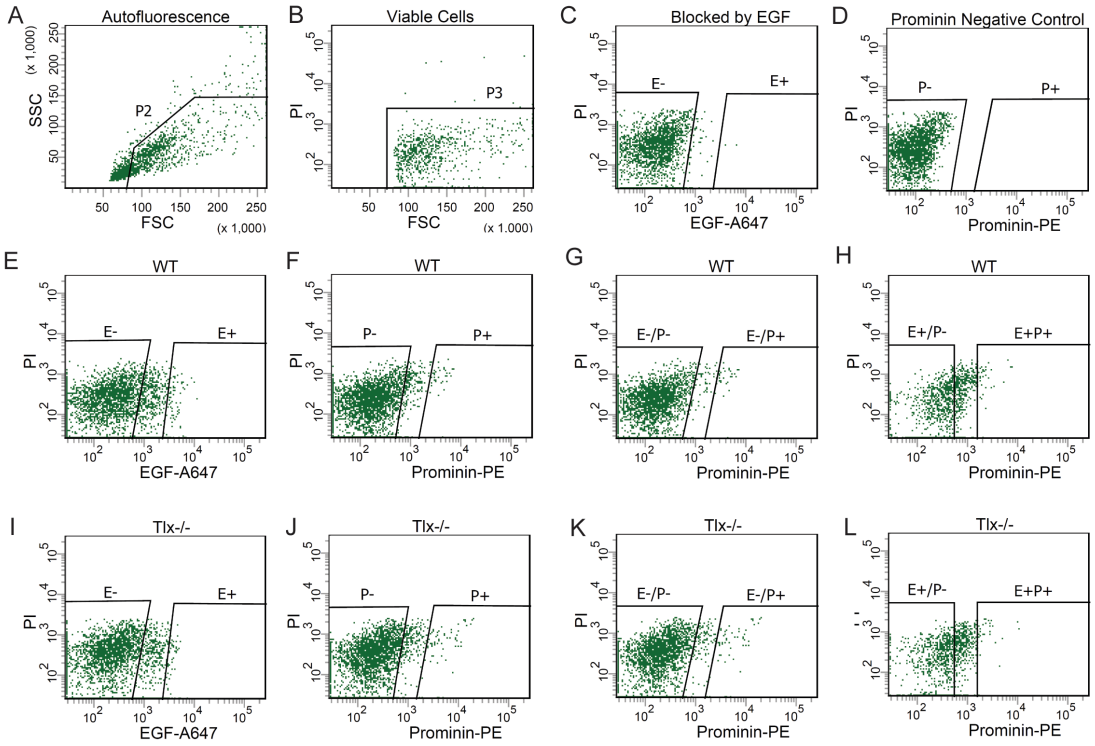

Figure 3.1 Representative gate settings of fluorescence activated cell sorting (FACS). The dissociated cells of the SVZ (P7) were stained with both Prominin-1-PE and EGF-Alexa647. The intact cell gate (P2) was set according to the autofluorescence control (A) as well as the viable cells gate (P3) was set by PI only staining (B). Meanwhile the EGFR (E- and E+) gates were set according to the control pre-blocked by EGF before EGF-Alexa647 single staining (C). The Prominin-1 negative gate (P-) was set based on a control with only PI staining (D) while the Prominin-1 positive gate (P+) based on both Prominin-1 and PI staining (F). The P+E-, P+E+, P-E+ and P-E- cells were sorted according to the intersectional gate settings of PE and Alexa647. Representative plots of these four populations in both WT (E, F, G, H) and KO (*Tlx*$^{-/-}$) (I, J, K, L) are shown.

By comparing the percentage of the four populations in WT and *Tlx*$^{-/-}$ neonatal mice (postnatal day 7, p7), I found that in the latter a higher percentage of P+E- cells, which consist of qNSCs and ependymal cells, and a concomitant decrease in the number of aNSCs (P+E+) and TAPs (P-E+) (Figure 3.2 A). These changes were not due to differences in cell viability among the

genotypes as, the percentage of dead cells between WT and *Tlx*$^{-/-}$ mice analysed, as indicated by PI staining, revealed no significant differences (Figure 3.2 B).

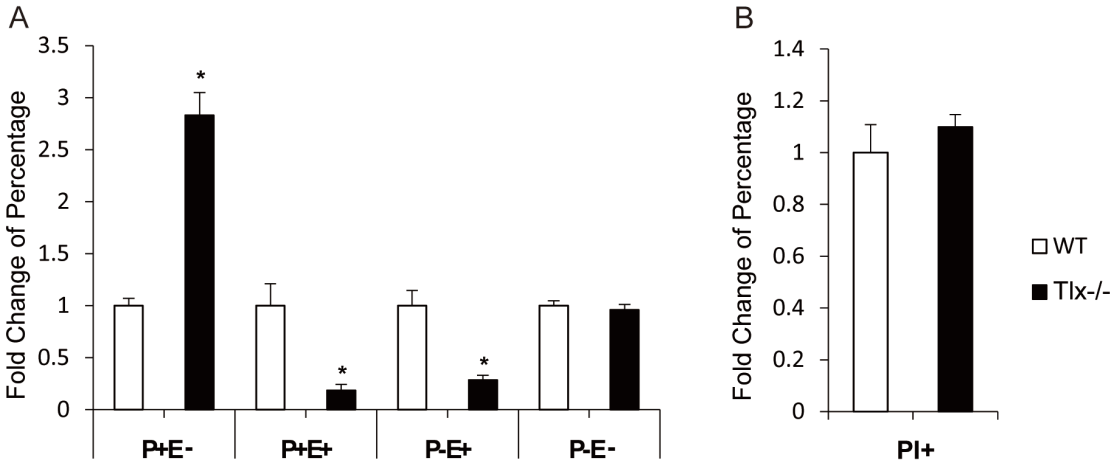

Figure 3.2 Neurogenesis is impaired in *Tlx*$^{-/-}$ mice. (A) The percentage of P+E- cells (qNSC) of *Tlx*$^{-/-}$ mice (P7) was increased while the P+E+ cells (aNSC) and P-E+ cells (TAPs) were decreased. (B) The percentage of PI+ cells was not significantly different between WT and *Tlx*$^{-/-}$ mice. (Data are presented as mean ± SEM. and n≥3. * indicate P values <0.05)

Taken together, these data showed that the *Tlx*$^{-/-}$ mice display a higher number of P+E- cells, which include quiescent NSCs with a concomitant depletion of proliferating aNSCs and TAPs. Since we have previously shown that NSCs are not depleted in the mutant SVZ (Obernier et al., 2011), these data suggest that lack of *Tlx* leads to an impairment of NSC activation.

3.1.2 Comparative analysis of MASH1 expression in the WT and *Tlx*$^{-/-}$ SVZ

Mash1 is a transcription factor that in the SVZ expressed in aNSCs and especially in intermediate progenitors and neuroblasts (Carrillo-Garcia et al., 2010; Khatri et al., 2014). We have previously shown that the gene expression of Mash1 is downregulated in mutant aNSCs at P7 (Obernier et al., 2011). To confirm the reduction in aNSCs and TAPs in the SVZ of adult *Tlx*$^{-/-}$ mice, we analyzed Mash1 expression at the protein level by using immunohistochemistry. The percentage of MASH1+ cells in the SVZ was greatly reduced throughout the mutant SVZ including the dorsal and the lateral region of the niche (Figure 3.3 A, B), underscoring the impairment of NSC activation and lineage progression in the SVZ of *Tlx*$^{-/-}$ mice.

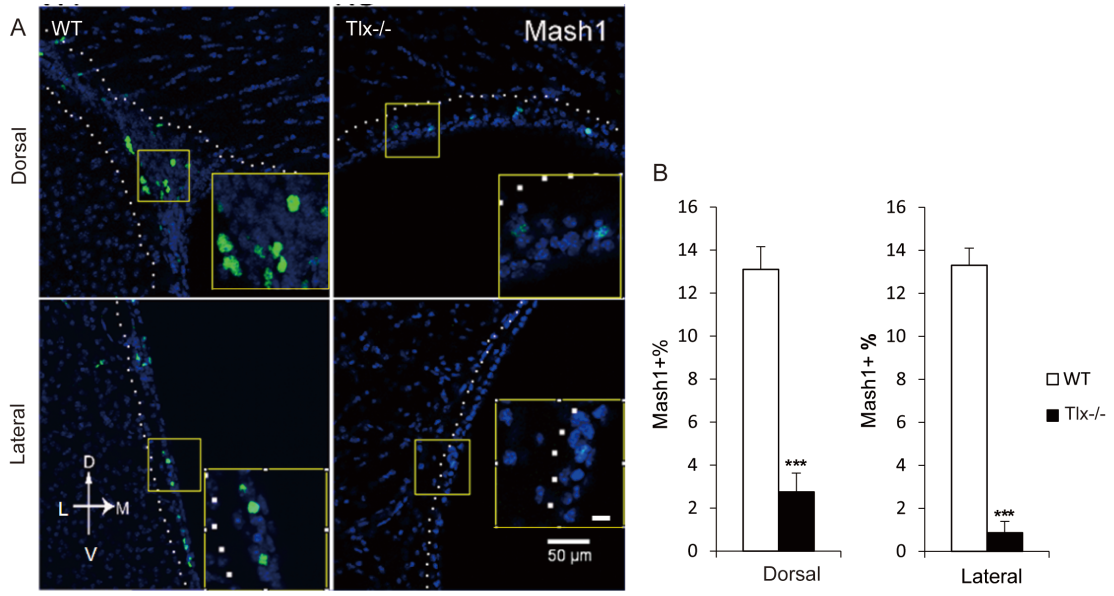

Figure 3.3 Percentage of MASH1+ cells decreases in *Tlx*$^{-/-}$ mice. The MASH1+ cells (Green) in both WT and KO were counted along the dorsal and lateral ventricle and the percentage of MASH1+ cells was calculated against DAPI stained nuclei (blue) of the indicated region by the dashed line. The representative staining is shown on the left (A) and the quantitative analysis is shown on the right (B) respectively. (Data are presented as mean ± SEM. and n≥3. *** indicate P values <0.001)

3.2 Gene expression profile of Notch signaling in WT and *Tlx*$^{-/-}$ mice

3.2.1 Gene expression profile in P+E-, P+E+, P-E+ and P-E- cells of the SVZ at P7

Adult neurogenesis is initiated only when qNSCs enter the cell cycle and become aNSCs. Therefore, to begin to investigate the mechanisms underlying the inability of mutant NSCs to enter the cell cycle, I next analyzed the gene expression profile changes of aNSCs between WT and *Tlx*$^{-/-}$ mice. We found that the *Mash1* mRNA was downregulated in aNSCs (P+E+)(Figure 3.4 A), which confirmed our previous findings and was consistent with the reduction in protein expression observed in adult *Tlx*$^{-/-}$ mice. More interestingly, we also found that Notch signaling effector genes *Hes1* and *Hes5* were significantly changed in aNSCs (P+E+)(Figure 3.4 B and C).

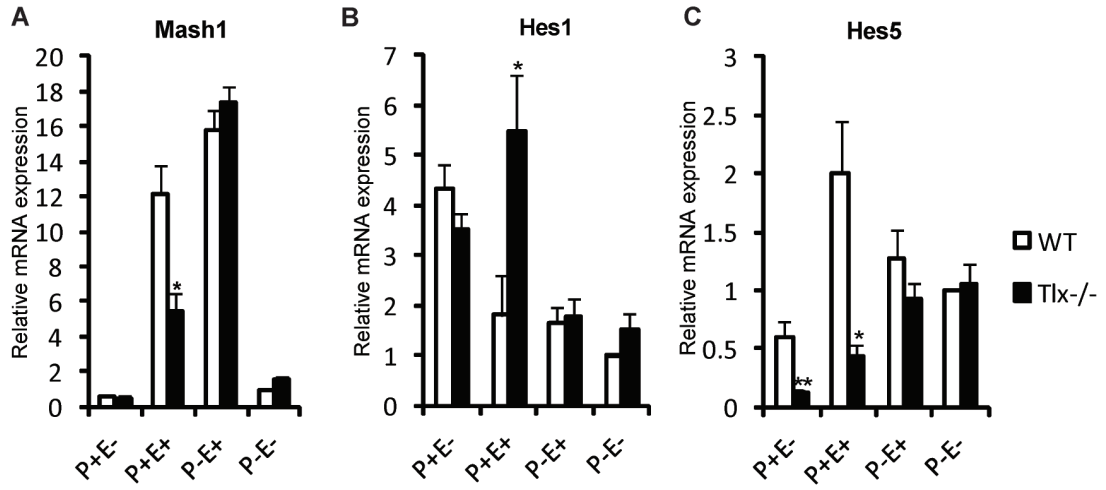

Figure 3.4 The gene expression profile of WT and *Tlx*$^{-/-}$ p7 mice. (A) *Mash1* expression is downregulated and (B) *Hes1* is upregulated in the aNSCs (P+E+) of *Tlx*$^{-/-}$ mice. (C) *Hes5* is downregulated in both qNSCs (P+E-) and aNSCs (P+E+). The fold changes of gene expression were normalized to WT P-E- cells (A, B, C) respectively. (Data are presented as mean ± SEM. and n≥3. * indicate P value <0.05, ** indicate P value <0.01)

Previous research showed that *Hes1* and *Hes5* compensate each other (Ohtsuka et al., 1999). Therefore, it is possible that the deregulation of *Hes1* (Figure 3.4 B) and *Hes5* (Figure 3.4 C) expression in opposite direction in aNSCs maybe an attempt to compensate an upregulation of Notch Signaling in the *Tlx*$^{-/-}$ niche. Intriguingly, *Hes5* is downregulated also in the qNSCs (P+E-), which implied that the Notch signaling is already altered in this cell population.

3.2.2 Comparative analysis of NICD1 positive cells in P+E- and P-E- of adult SVZ

Since the expression of Notch signaling molecules is upregulated in the SVZ of *Tlx*$^{-/-}$ mice, I next investigated whether the activated form of Notch1, NICD1 (Notch1 intercellular domain) is also upregulated in the adult SEZ. Therefore, after staining for Prominin-1 and EGFR and sorting the four populations from the adult SVZ, cells were plated on coverslips and stained with NICD1 antibody. Since EGFR^{high} cells are very few in *Tlx*$^{-/-}$ adult mice, aNSCs and TAPs could not be analyzed. And these experiments were performed only to compare P+E- and P-E- cells. Two different patterns of NICD1 immunostaining were detected. In some cells the immunoreactivity colocalized with the DAPI counterstaining of the nuclei, indicating a late stage of activated Notch signaling, where NICD1 is already translocated into the nucleus (Figure 3.5 A). In contrast, in its early activated, poised NICD1 is located close at the

membrane of the nucleus (Figure 3.5 B) (Andersson et al., 2011). Quantification of the immunostainings revealed that (Figure 3.5 C), independent of the genotype, around 30% of P+E- cells displayed either nuclear or perinuclear NICD1 immunoreactivity (NICD1+) and only 40% were NICD1-, underscoring the importance of Notch signaling in the regulation of NSC quiescence. The absence of a significant difference in the distribution of NICD1 between WT and *Tlx*$^{-/-}$ P+E- cells was surprising (Figure 3.5 D), but it could be a consequence of the involvement of other Notch receptors, which could not be detected by the antibodies used here. However, I found that the percentage of nuclearized NICD1 in the population of *Tlx*$^{-/-}$ P-E- cells was significantly higher than in the WT counterpart (Figure 3.5 E). As it was reported that the P-E- population includes a minor subset of NSCs (Codega et al., 2014; Walker et al, 2013), this results suggest an upregulation of Notch1 signaling in this population of NSCs.

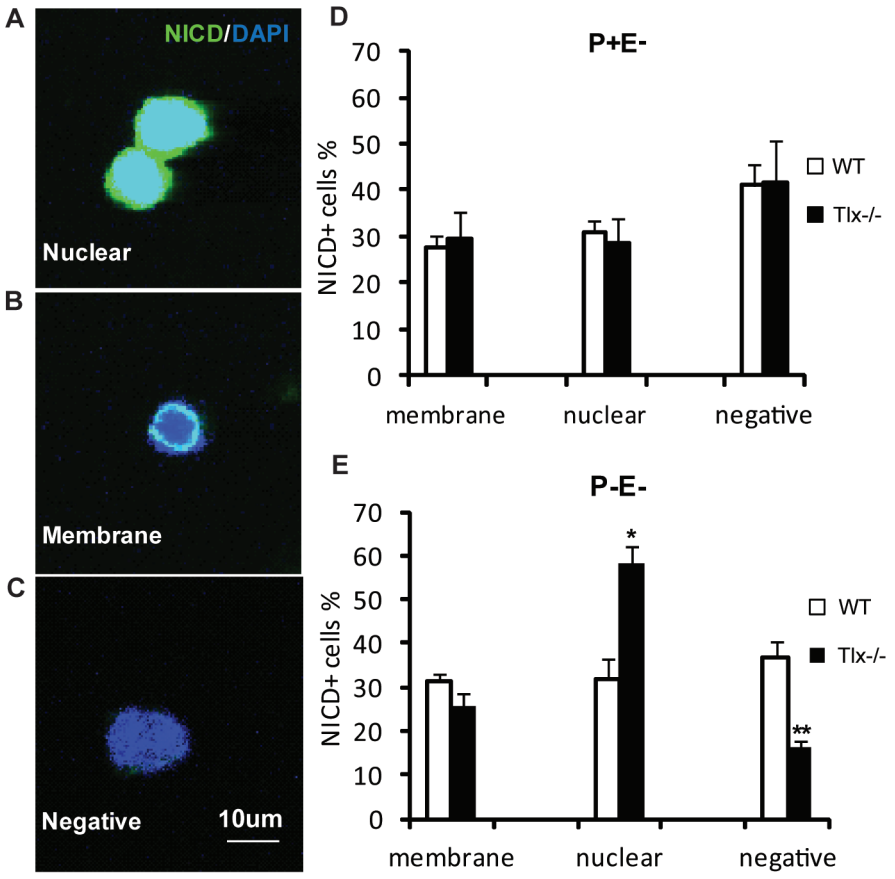

Figure 3.5 Comparative analysis of NICD1 staining in the adult SVZ in P+E- and P-E- populations. Representative pictures of NICD1 staining of sorted cells show that activated Notch1 in the nuclear (A), nuclear membrane (B) or negative (C). The percentage of NICD1+ cells in WT and *Tlx*$^{-/-}$ (D, E) are shown at right. (Data are presented as mean ± SEM. and n≥3. * indicate P values <0.05; ** indicate P values <0.01)

3.2.3 Comparative analysis of gene expression in NSCs derived from the dorsal and lateral SVZ

As illustrated above (Figure 3.3 A), most of the MASH1+ cells were located at the corner formed by the junction between the dorsal and the lateral part of the germinal niche, indicating more active neurogenesis in this region. NSCs in dorsal and lateral regions of the ventricles have a distinct differentiation potential (Young et al., 2007), indicating that they represent two pools of functionally distinct NSCs. Therefore, I next used differential dissection to separate the dorsal and lateral pools of NSCs in the WT (Figure 3.6 A) and *Tlx*$^{-/-}$ (Figure 3.6 A') SVZ.

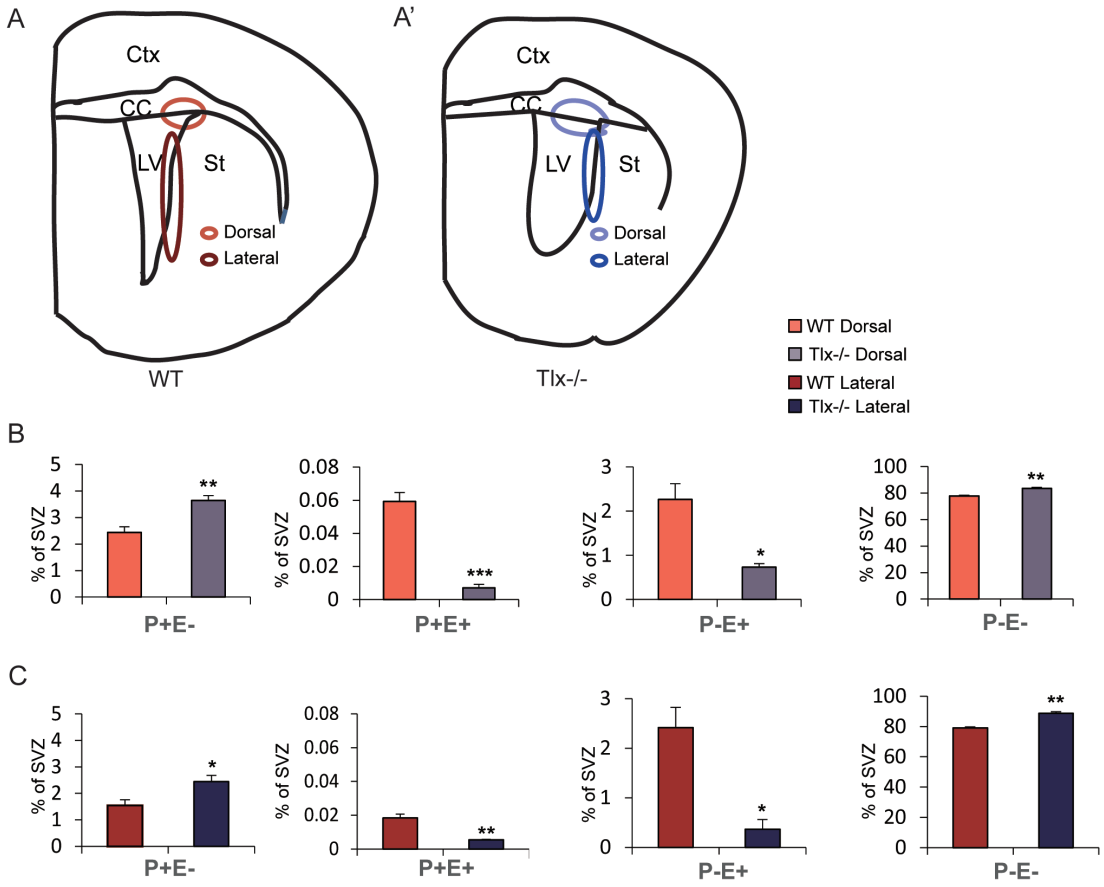

Figure 3.6 Comparative analysis of NSCs compositions in dorsal and lateral regions of SVZ. The scheme (A, A') shows the defined regions of SVZ in WT and *Tlx*$^{-/-}$, respectively. In the *Tlx*$^{-/-}$ mice the percentage of qNSCs increased while the aNSCs and TAPs decreased in both dorsal (B) and lateral (C) regions. (Data are presented as mean ± SEM. and n≥3. * indicate P values <0.05; ** indicate P values <0.01; *** indicate P values <0.001)

Consistent with the previous analysis of the total SVZ, I found an enrichment of qNSCs (P+E-) with a concomitant depletion of aNSCs (P+E+) and TAPs (P-E+) in both dorsal and lateral regions of the *Tlx*$^{-/-}$ niche, indicating that the effect of *Tlx* on NSCs quiescence is not affected

by regional cues (Figure 3.6 B and C).

To investigate whether the Notch signaling is involved in regulating the NSC maintenance in *Tlx*$^{-/-}$ mice, I analyzed the expression profile of genes involved in Notch signaling in qNSCs (P+E-) sorted from the dorsal and lateral ventricle of neonatal WT and *Tlx*$^{-/-}$ mice (P7) (Figure 3.7).

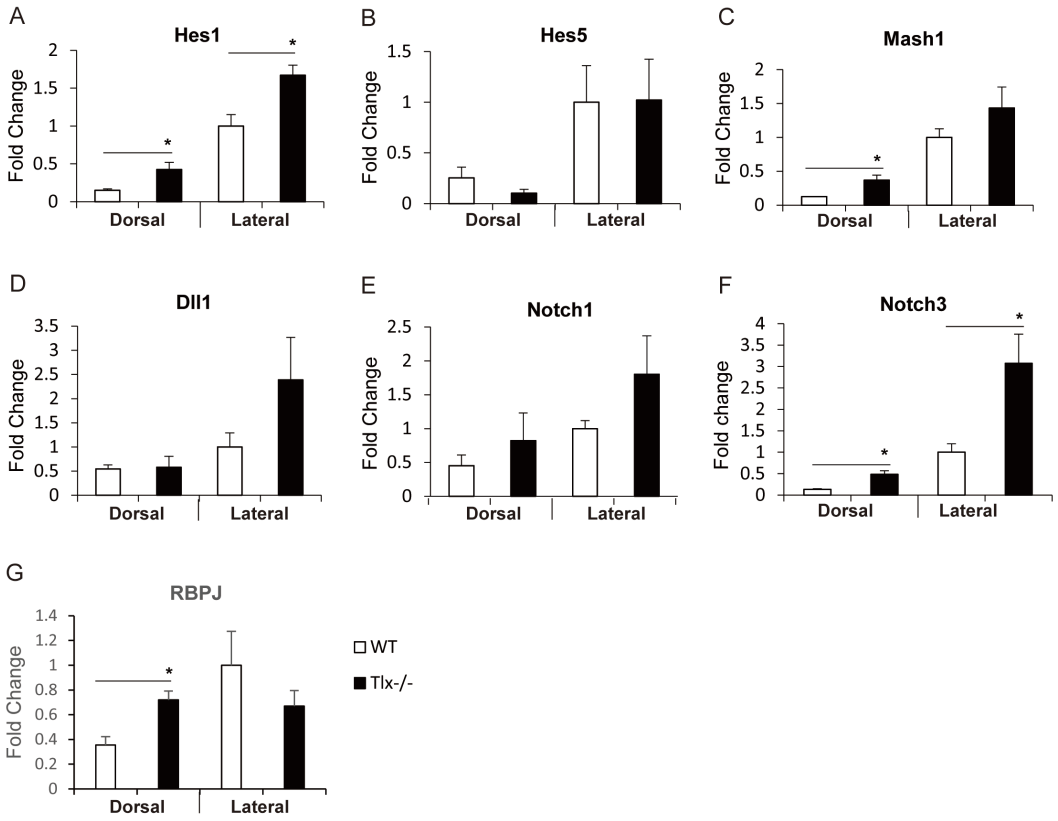

Figure 3.7 Notch signaling upregulated in qNSC (P+E-) of *Tlx*$^{-/-}$ niche. The gene expression profile of Notch signaling genes *Hes1* (A), *Hes5* (B), *Mash1* (C), *Dll1* (D), *Notch1* (E), *Notch3* (F) and *RBPJ* (G) in both dorsal and lateral region. (Data are presented as mean ± SEM. and n≥3. * indicate P value <0.05)

I found that compared to the WT counterparts *Notch3* but not *Notch1* was significantly upregulated in *Tlx*$^{-/-}$ qNSCs (Figure 3.7 E and F). The Notch effector gene *Hes1* was also upregulated in both dorsal and lateral qNSCs (Figure 3.7 A), which was previously failed to distinguish by combining the dorsal and lateral qNSCs together. In contrast, the *RBPJ* and *Mash1* were upregulated only in the dorsal region of niche (Figure 3.7 G and C), indicating a different gene expression profile between regionally distinct qNSCs. RBPJ is a molecular switch, which could initiate the expression of *Hes1* upon NICD binding (Ables et al., 2011).

This suggests that the NICD-RBPJ signaling cascade underlies the activation of *Hes1* in the dorsal region. Nevertheless, in the lateral region, it is still unclear how NICD-RBPJ signaling is involved in upregualting the *Hes1* expression. Surprisingly, the *Mash1* was also upregulated in the dorsal *Tlx*$^{-/-}$ qNSCs (Figure 3.7 C) although the overall expression level was very low compared to those observed in TAPs (Figure 3.4 A). This may imply that in qNSCs the *Mash1* upregulation was favored by the *Tlx* mutation. Finally, there was no significant difference in the expression of *Notch1*, *Dll1* and *Hes5* in qNSCs (P+E-) between WT and *Tlx*$^{-/-}$ mice (Figure 3.7 E, D and B).

I next performed a similar analysis in the P-E- population of neonatal *Tlx*$^{-/-}$ mice (Figure 3.8). Interestingly, I found that Notch signaling effector gene *Hes1* was also upregulated in both corner and lateral region of *Tlx*$^{-/-}$ mice (Figure 3.8 A), which confirmed our finding about NICD1 staining in adult P-E- cells (Figure 3.5 E). Moreover, in P-E- isolated from the lateral SVZ of *Tlx*$^{-/-}$ mice, transcripts for *Hes5* were also upregulated (Figure 3.8 B). Although Notch receptors *Notch1* and *Notch3* were not upregulated in the dorsal region (Figure 3.8 E and F), one of the very important ligand for *Notch1* the *Dll1* gene was significantly upregulated in this region of *Tlx*$^{-/-}$ mice (Figure 3.8 D). In contrast, the genes *Mash1* and *RBPJ* were not significantly different in their expression between WT and *Tlx*$^{-/-}$ mice (Figure 3.8 C and G).

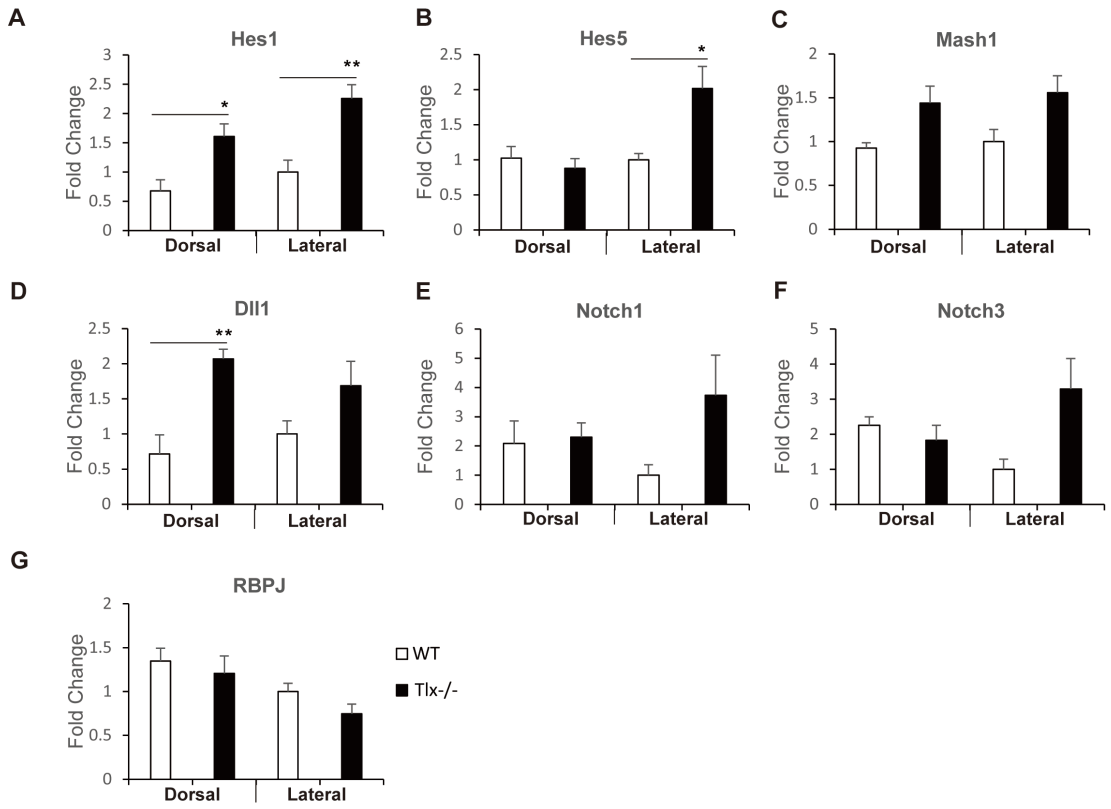

Figure 3.8 Notch signaling is upregulated in P-E- cells of the *Tlx*$^{-/-}$ niche. Gene expression profile of Notch signaling genes *Hes1* (A), *Hes5* (B), *Mash1* (C), *Dll1* (D), *Notch1* (E), *Notch3* (F) and *RBPJ* (G) in both dorsal and lateral region. (Data are presented as mean ± SEM. and n≥3. * indicate P values <0.05; ** indicate P values <0.01)

3.3 *In Vivo* modulation of Notch signaling by DAPT

3.3.1 The proliferation of NSCs in SVZ increases after DAPT treatment

I found that the *Tlx*$^{-/-}$ mice have upregulated Notch signaling and impaired neurogenesis. Since Notch signaling has been shown to promote cell quiescence in the adult SVZ (Chapouton et al., 2010), the increase in qNSCs maybe a consequence of increased Notch signaling. Therefore, I reasoned that the impaired neurogenesis in *Tlx*$^{-/-}$ mutants may be rescued by inhibitors of the Notch signaling (Figure 3.9 A). To verify this hypothesis *in vivo*, I injected the Notch Inhibitor DAPT (10mM) and the vehicle control DMSO into the right and left ventricles respectively of adult WT and *Tlx*$^{-/-}$ mice. After 24 hours the mice were sacrificed and brain slices were immunostained with Ki67 antibodies to analyze the effect of the injection on the number of cycling cells. The percentage of Ki67 positive (Ki67+) cells was significantly increased in the dorsal region of DAPT treated ventricle in both WT and *Tlx*$^{-/-}$ mice (Figure 3.9 B and C),

showing that that qNSC could re-enter the cell cycle upon inhibition of Notch signaling.

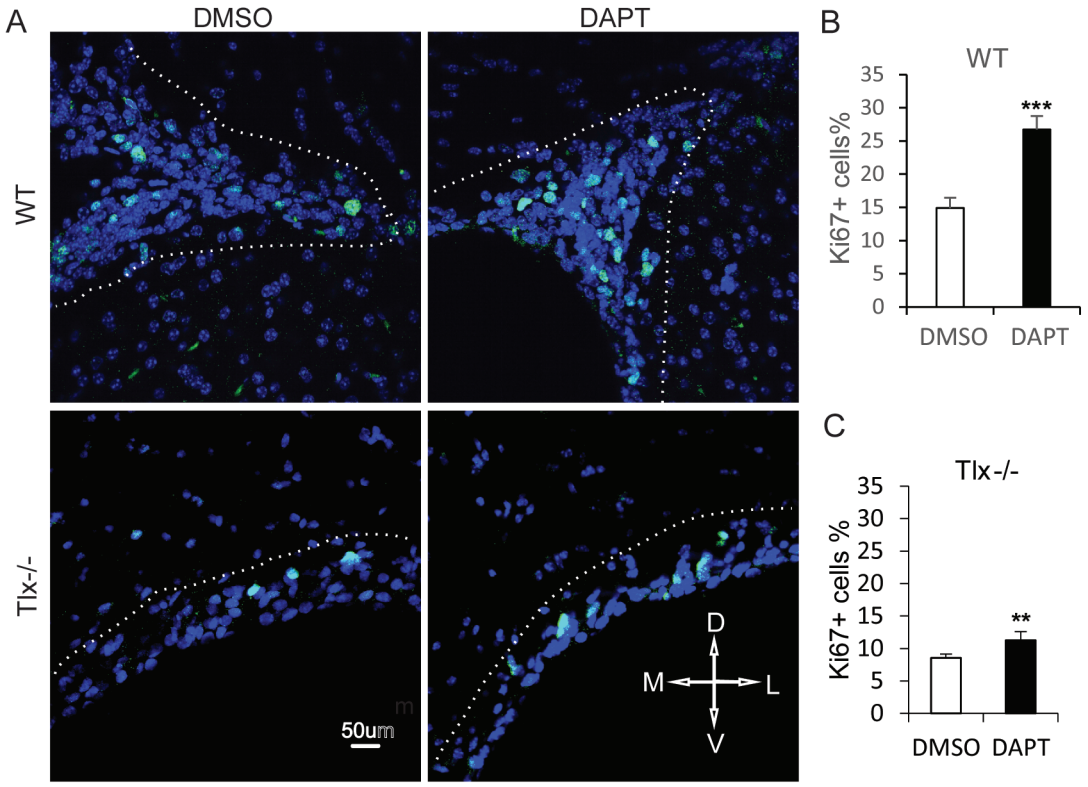

Figure 3.9 Proliferation of NSCs in SVZ increases after DAPT treatment. The Ki67+ cells (Green) in both WT and *Tlx*$^{-/-}$ were counted along the dorsal line of ventricle and the percentage of Ki67+ cells was calculated against DAPI stained nuclei (blue) of the indicated region by the dashed line. Representative staining is shown (A) and the calculation (B, C), respectively. (Data are presented as mean ± SEM. and n≥3. ** indicates P values <0.01; *** indicate P values <0.001)

3.3.2 Identification of the cell types affected by DAPT treatment

To find out which precursor type is affected by the blockade of Notch signaling, I injected mice intraventricularly with DMSO and DAPT as illustrated above (Figure 3.9 A). After 24 hours mice were sacrificed and processed for FACS sorting to isolate the four cell populations. Surprisingly, I found that the treatment led to an increase in the percentage of P+E- cells (qNSCs) in both WT and *Tlx*$^{-/-}$ SVZ. In contrast, the percentage of aNSCs was only increased in WT mice (Figure 3.10 A and B). Moreover, *Tlx*$^{-/-}$ mice displayed a small but significant decrease in the number of P-E- cells after exposure to DAPT. To identify which cell types upregulate Ki67 expression, after sorting cells were plated and processed for Ki67 immunostaining (Figure 3.10 C and D). This analysis revealed that the treatment induced no change in the percentage of Ki67+ cells in the various cell population isolated from WT mice

(Figure 3.10 C). Taken together, the data of the FACS analysis show that the increase in the number of Ki67+ cells observed in situ in the WT SVZ is a consequence of the increase in the total number of P+E- and P+E+ cells displaying Ki67 immunoreactivity. In the mutant SVZ the percentage of Ki67+ cells also did not vary among the various populations with the exception of the P-E- cells, which displayed a small but significant increase in the percentage of Ki67+ cells (Figure 3.10 D). These data suggest that the increase in the number of Ki67+ cells observed in *Tlx*$^{-/-}$ slices is a consequence of the increase in the total number of P+E- cells and P-E- cells displaying Ki67 immunoreactivity. They also show that *in vivo* blockade of Notch signaling is not sufficient to rescue the transition of mutant P+E- qNSCs to P+E+ aNSCs.

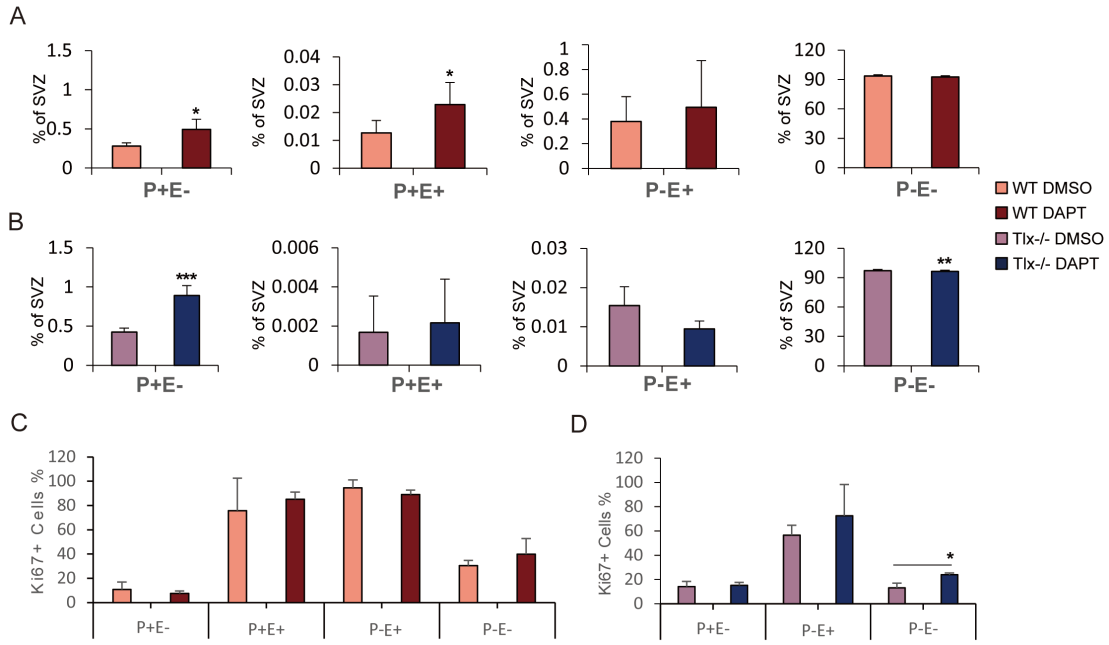

Figure 3.10 Comparative analysis of populations in the adult SVZ after DAPT treatment. The percentage of qNSC and aNSC was increased in the DAPT injected ventricle of WT (A). The percentage of qNSC was increased and P-E- cells were decreased in the DAPT injected ventricle of *Tlx*$^{-/-}$ mice (B). The percentage of Ki67+ cells did not change after DAPT injection (C, D) but in the P-E- population of *Tlx*$^{-/-}$ mice (D). (Data are presented as mean ± SEM. and n≥3. * indicate P values <0.05; ** indicate P values <0.01; *** indicate P values <0.001)

3.3.3 Inhibition of Notch signaling promotes P-E- cells to be P+

My previous analysis shows that in both WT and in mutant mice the total number of P+E- cells almost doubles 24 hours after DAPT treatment without a concomitant increase in the proportion of Ki67+ cells. This suggests that some of the P-E- cells may become P+E- cells upon Notch inhibition. This hypothesis is consistent with previous findings (Wang et al., 2008).

It is also consistent with my observations that a subset of mutant P-E- cells display over activation of Notch signaling (Figure 3.5 E), that in the *Tlx* mutant SVZ the percentage of P-E- cells which are cycling increases whereas the total number P-E- cells decreases upon DAPT treatment.

To further investigate this hypothesis, I sorted the P-E- cells of adult WT and *Tlx*$^{-/-}$ mice by FACS. Thereafter the cells were cultured in the presence of either vehicle (DMSO), 20 μM or 40 μM DAPT in FGF2 containing medium for one day *in vitro*. Then, the cells were stained with Prominin-1 for analysis (Figure 3.11).

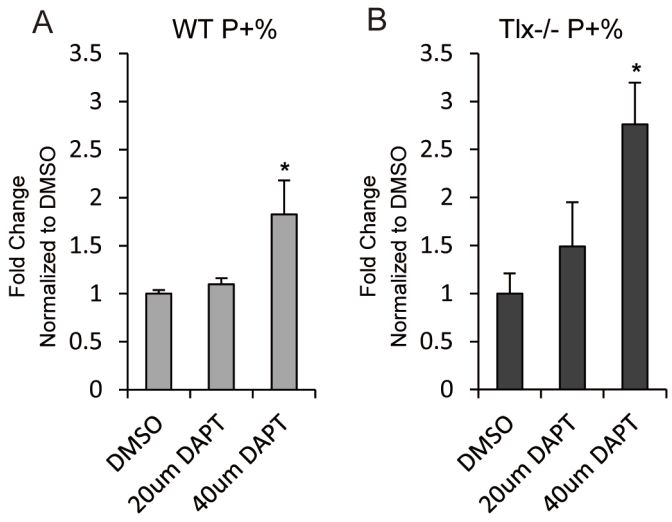

Figure 3.11 Inhibition of Notch signaling promotes P-E- cells to become P+ cells. The P-E- cells sorted from both WT and *Tlx*$^{-/-}$ adult mice were cultured for 1 day before FACS analysis of Prominin-1 staining. The percentage of P+ cells was significant increased in the presence of 40 μM DAPT in both WT (A) and *Tlx*$^{-/-}$ (B). (Data are presented as mean ± SEM. and n≥3. * indicate P values <0.05)

The percentage of P+ cells was increased when the cells were cultured in presence of 40 μM DAPT in both WT and especially *Tlx*$^{-/-}$ cultures (Figure 3.11 A, B). These data suggest that there is a subset of cells in the P-E- population, which may re-establish the expression of stem cell marker Prominin-1 when Notch signaling is blocked.

3.4 TLX represses Notch effector gene *Hes1* and *Hes5*

3.4.1 TLX represses transcription of *Hes1* and *Hes5*

To analyze how TLX regulates expression of *Hes1* and *Hes5*, I took advantage of a luciferase

assay. To this end, I used plasmids that the promoters of *Hes1* and *Hes5* were cloned upstream of the Luciferase reporter gene respectively (Figure 3.12 A) (Nishimura et al., 1998) and co-transfected constructs with either an empty plasmid (FUGW) as control or a plasmid driving TLX (Tlx) expression. Quantitative analysis revealed that overexpression of TLX repressed the activity of both *Hes1* and *Hes5* promoters (Figure 3.12 B). This inhibitory effect of TLX was not observed if the RBPJ binding site of the *Hes1* promoter was deleted, indicating that the repressive effect of TLX on *Hes1* transcription is dependent on this sequence which is very important for Notch signaling. Co-transfection of a plasmid overexpressing the activated form of Notch1 (NICD1, Dang et al., 2006) led to two folds increase of *Hes1* promoter and twelve folds increase of *Hes5* promoter reporter activity, respectively (Figure 3.12 D). Even in the presence of NICD1 overexpression, *Hes1* and *Hes5* were still both repressed in the presence of the *Tlx* coding plasmid. The removal of the RBPJ site from Hes1 promoter revealed a slightly activation after cotransfection of NICD1, which suggests that the RBPJ site is important for the interaction of TLX on the *Hes1* promoter (Figure 3.12 D). To verify the interaction of TLX at the RBPJ binding site, an artificial promoter which contains ten copies of RBPJ binding sites along with an *adTATA* mini promoter was cloned upstream of Luciferase reporter gene (Mckenzie et al., 2006). There was eight folds increase of the reporter activity when *Tlx* was overexpressed instead of the empty plasmid FUGW (Figure 3.12 C). As control we used a plasmid containing only *adTATA* mini promoter. Surprisingly, there was also three folds increase when only *adTATA* mini promoter was used, hinting the possibility of more complex protein-interactions of TLX with transcriptional coregulators. The luciferase activity of the plasmid 10XRBPJ-adTATA was greatly increased when NICD1 was cotransfected, which showed as expected that the RBPJ sites have a strong interaction with NICD1-RBPJ complex. However, the interaction between TLX and RBPJ sites were masked by highly activated Notch signaling with overexpressing NICD1 as there was no significant repression upon TLX overexpression (Figure 3.12 E).

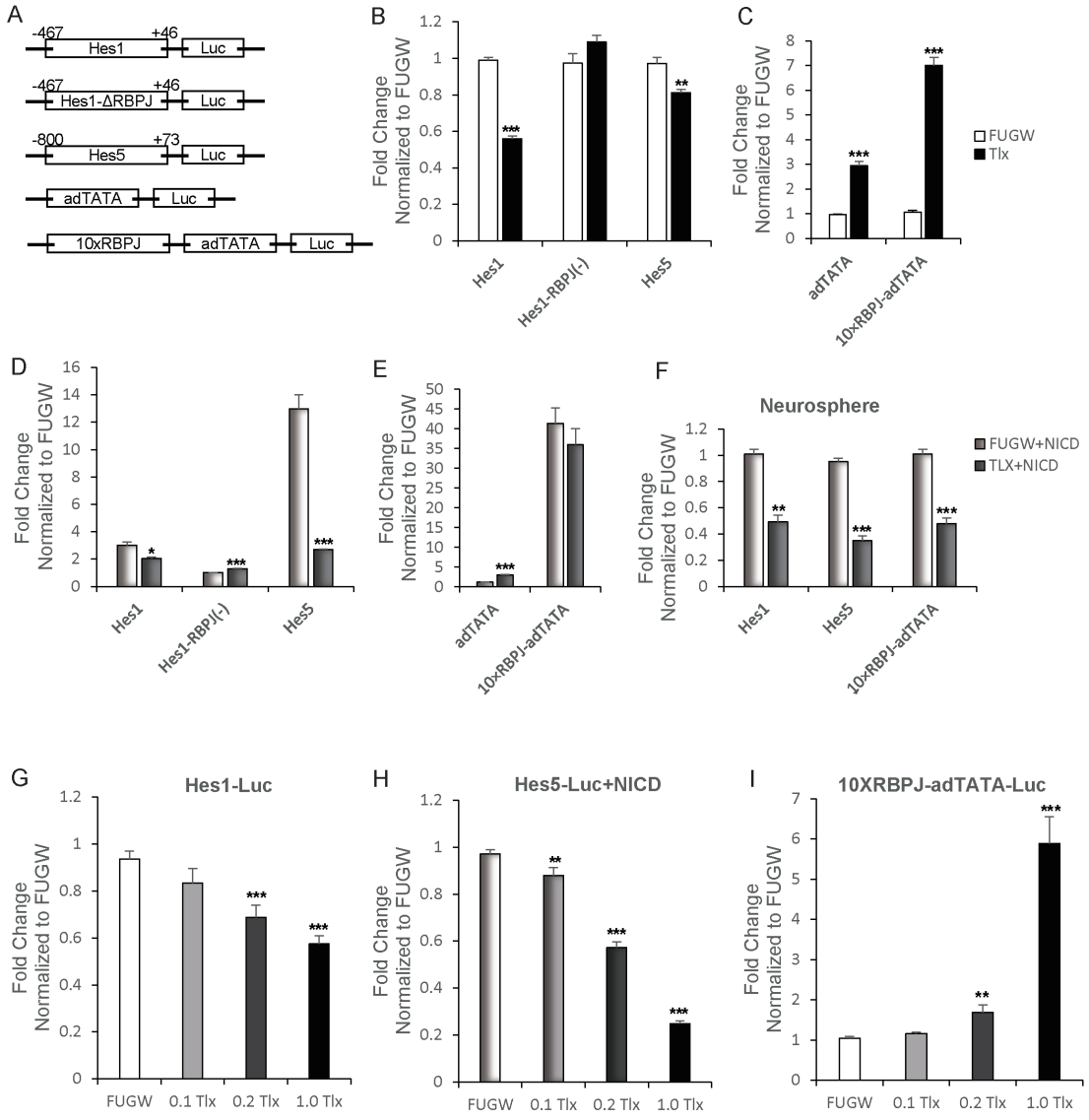

Figure 3.12 TLX represses transcription of *Hes1* and *Hes5*. (A) Scheme of the luciferase reporter plasmids. The Luciferase activity of *Hes1* and *Hes5* promoter were decreased by TLX overexpression with (D) or without (B) cotransfected NICD1 in HEK293 cells. The luciferase activity of the promoter with 10 repeats of the RBPJ binding site was increased by TLX overexpression (C) but decreased when cotransfected with NICD1 (E) in HEK293 cells. The repression of TLX on *Hes1/5* transcription was confirmed in neurosphere cultures (F). The repression of *Hes1/5* transcription and the interaction to RBPJ sites was TLX dose-dependent (G, H, I). [10% (0.1Tlx), 20% (0.2Tlx), 100% (1.0 Tlx) of the amount of FUGW]] (Data are presented as mean ± SEM. and n≥3. * indicate P values <0.05; ** indicate P values <0.01; *** indicate P values <0.001)

The HEK293 cells are derived from human embryonic kidney cells and represents a heterologous system, which may introduce experimental artifacts. Therefore, I next performed similar experiments in cultivated neurospheres isolated from the SVZ of adult WT mice. Confirming the differences between the two experimental setups endogenous Notch signaling

was different between the two systems (HEK293 cells and neurosphere cells). However, also in neurosheres I was able to confirm the repression of *Hes1/5* by TLX in the presence of forced Notch activation (NICD1 overexpression) (Figure 3.12 F). Moreover, the repression of *Hes1* and *Hes5* promoters by TLX (Figure 3.12 G and H) as well as the interaction of TLX with the RBPJ sites (Figure 3.12 I) both increased with the amount of the transfected construct coding for TLX, which likely reflected increasing amounts of TLX protein.

3.4.2 TLX represses *Hes1/5* expression by interacting to RBPJ sites at their promoters

To verify the interaction of TLX with the promoters of *Hes1* and *Hes5* I performed Chromatin Immunoprecipitation (ChIP) assays in cultivated neurospheres. In Figure 3.13 A is shown the region flanked by the primers used for amplification of the DNA fragment containing the RBPJ sites in both genes. The DNA fragment from the *Hes1* and *Hes5* promoters were enriched when the protein/DNA complex was precipitated by TLX antibody but not unspecific rabbit IgG antibody (Figure 3.13 B and C). Both promoters revealed a significant enrichment of TLX at the RBPJ site of *Hes1* and *Hes5*, which indicates that the regulation by TLX is dependent on either a direct interaction of the orphan nuclear receptor with the RBPJ or with the transcriptional complex assembled at this site.

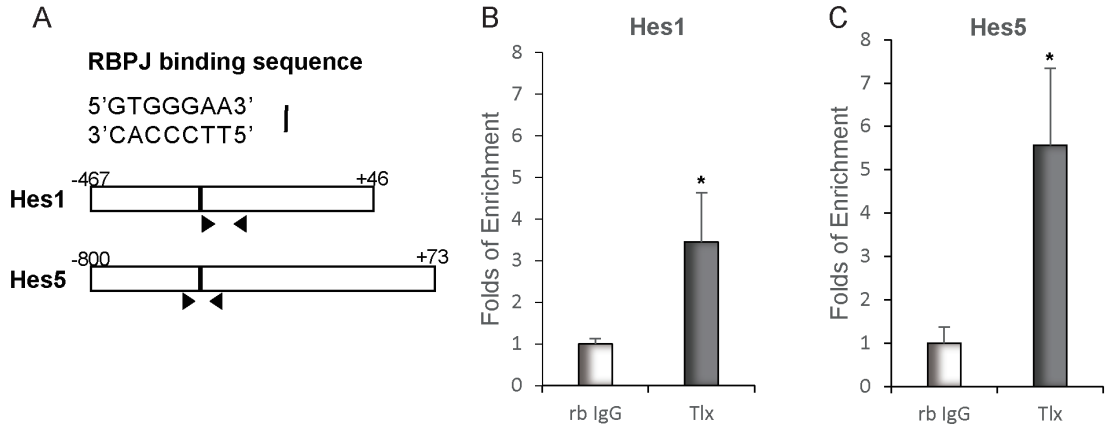

Figure 3.13 TLX represses *Hes1/5* expression by binding to RBPJ sites of their promoters. (A) Scheme of the primers amplifying region and RBPJ binding site. The fold enrichment of TLX precipitated promoter region of interest in *Hes1* (B) and *Hes5* (C) compared to unspecific rb IgG (normal rabbit IgG) are shown. (Data are presented as mean ± SEM. and n≥3. * indicate P value <0.05)

3.5 Knocking down *Hes1* cannot rescue the quiescence of P+E- cells

My results have shown that TLX represses the expression of *Hes1* in neural precursors and that Hes1 expression is upregualted in both mutant P+E- and P+E- cells. Moreover, my data suggest that blocking Notch signaling in vivo promotes the proliferation of P-E- precursors and their transition to P+E- cells. However, blockade of Notch signalling per se was not enough to rescue the transition of P+E- qNSCs to P+E+ aNSCs. Therefore, I next investigated whether a decrease in *Hes1* expression may rescue the impairment in the proliferation of neural precursors. To test this hypothesis, I took advantage of clonal assays to determine the effect of *Hes1* expression levels on the clone forming ability of either precursor group. After sorting P+E- and P-E- cells were infected with AAV either carrying a scramble shRNA or *Hes1* shRNA after sorted from SVZ of adult mice. The cells were cultivated in the presence of EGF and hFGF2 for four weeks and clone formation was checked every week. I found that the treatment did not significantly affect the clone formation ability of P+E- cells, which independently of the genotype and the transduction regime did not form big clones, indicating that the quiescence could not be rescued by merely knocking down *Hes1* in this cell population. Downregulation of Hes expression also did not affect significanty clone formation of WT P-E- cells (Figure 3.14 A). However, around 0.004% cells formed clones in the *Tlx* mutant P-E- cells upon transduction with *Hes1* shRNA, showing that increased Hes1 following *Tlx* deletion promotes quiescence in this cell population (Figure 3.14 B).

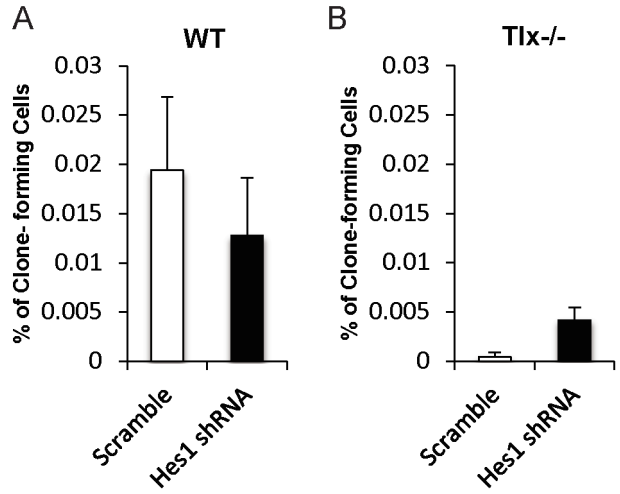

Figure 3.14 Clonal analysis of P-E- cells infected with AAV. The P-E- cells were infected with AAV either carrying a scramble shRNA or *Hes1* shRNA immediately after sorting. The clones were counted 1-2 weeks after infection in both WT (A) and *Tlx*$^{-/-}$ (B). (Data are presented as mean ± SEM. and n≥3.

4. Discussion

4.1 Neurogenesis is impaired in *Tlx*$^{-/-}$ mice

Previous observations have already shown that *Tlx*$^{-/-}$ mice have greatly expanded lateral ventricles, severely reduced hippocampal dentate gyri and reduced olfactory bulbs (Monaghan et al. 1997), indicating an impairment of adult neurogenesis. To investigate the cellular dynamics underlying the effect of Tlx mutant, our group has previously shown that such an impairment of neurogenesis progressively increases from late development into adulthood (Obernier et al., 2011). It was also shown that this reflected a progressive decrease in the number of E+(EGFR^{high}) cells in the mutant SEZ, which include aNSCs and TAPs. This ultimately results in the complete absence of E+ cells in the adult mutant SVZ. Finally it was found that such a dramatic reduction of E+ cells was due to an arrest of NSCs in quiescent status that could be reversed by re-establishment of *Tlx* expression (Niu et al., 2011).

Extending these previous observations I here found that aNSCs and TAPs were dramatically decreased also in the SVZ of adult *Tlx*$^{-/-}$ mice. This conclusion was confirmed by quantification of MASH1 expressing cells in the WT and mutant SVZ. The proneural gene *Mash1* (*Ascl1*) is a bHLH (basic helix-loop-helix) transcription factor highly expressed in EGFR positive SVZ cells (Obernier et al., 2011; Khatri et al., 2014). My immunohistochemical analysis revealed not only a decreased number of MASH1+ cells in *Tlx*$^{-/-}$ mice (Figure 3.3 B), but also possible regional cues, further affecting the neurogenesis in the mutant SVZ. Whereas the percentage of MASH1+ cells were the same in both dorsal and lateral regions of the WT SVZ, almost no MASH1+ cells were found in the lateral region of *Tlx*$^{-/-}$ mice (Figure 3.3 A), which suggested a different spatial regulation of NSCs. This was indeed confirmed by the analysis of the different populations (P+E-, P+E+, P-E+, P-E-) in these two regions between WT and *Tlx*$^{-/-}$ mice, showing that the number of TAPs was more affected by the lack of *Tlx* in the lateral than in the dorsal SVZ (Figure 3.6 B and C). Consistent with this I also found in situ that the few remaining cells displaying MASH1 or Ki67 immunoreactivity were localized at in the dorsal SVZ (Figure 3.3 and Figure 3.9 respectively). Taken together, these data confirmed a reduction of aNSCs in the *Tlx*$^{-/-}$ mice. Interestingly, it was recently shown that that TLX can activate *Mash1* to

induce the neuronal lineage commitment of NSCs (Elmi et al., 2010), suggesting that the depletion of E+ cells might be a consequence of decreased levels of *Mash1* expression following *Tlx* ablation.

4.2 Notch signaling is upregulated in the absence of TLX

To further investigate the molecular mechanisms of impaired neurogenesis in *Tlx*$^{-/-}$ mice, I compared the gene expression profile of both WT and *Tlx*$^{-/-}$ mice (Figure 3.4). Interestingly, I found that Notch signaling effector genes *Hes1* and *Hes5* were both significantly altered in aNSCs (P+E+), albeit in opposite directions highlighting a potential compensatory mechanism between Hes1 and Hes5 as previously described (Ohtsuka et al., 1999). In these experiments values of transcript levels for each population were normalized to the ones of the WT P-E-, which was selected as the reference value. This approach allowed me to visualize the changes in expression levels of each gene at each stage of lineage progression, and highlighted again opposite trends of expression of the two genes in WT precursors. Whereas *Hes1* is mainly expressed in the population of P+E- cells and it decrease in proliferating populations (Figure 3.4 B), *Hes5* is mostly expressed in aNSCs (Figure 3.4 C). Nevertheless, with this type of analysis I could not detect a change of *Hes1* gene expression in the population of qNSCs, which was only detected upon direct comparison of WT and *Tlx*$^{-/-}$ P+E- cells. Although there is no difference of NSC composition in the dorsal and lateral regions of SVZ, NSCs from these two regions have different neurogenic fates due to their different embryonic origin (Young et al., 2007). For this reason, I compared the gene expression profile in qNSCs (P+E-) in these two regions separately (Figure 3.7). Interestingly, the *Hes1* was upregulated in both the dorsal and lateral portion of the *Tlx*$^{-/-}$ SVZ. The expression of *Hes1* and *Hes5* in the lateral SVZ was much higher (more than two folds) than in the dorsal region (Figure 3.7 A and B). Moreover, independent of the genotype, the Notch ligand *Dll1* and Notch receptors *Notch1* and *Notch3* were also expressed at a higher level in lateral than in the dorsal SVZ (Figure 3.7 D, E and F). On the other hand, it means that the high level of Notch signaling is inversely related to the proliferative capability. Interestingly, the Notch receptor *Notch3* but not *Notch1* was increased significantly in *Tlx*$^{-/-}$ qNSCs (P+E- cells). Alunni et.al showed that

Notch3 signaling is also very important for gating the activation of NSCs (Alunni et al., 2013). Moreover, Basak et.al showed that aNSCs but not qNSCs are Notch1-dependent which is consistent with our finding (Basak et al., 2012). Interestingly, it was found that in the *Notch1*$^{-/-}$ *Drosophila* embryo, the expression of Hes5 is reduced while the Hes1 is not (de la Pompa et al., 1997). Taken together, my data suggest that the quiescence of NSCs in *Tlx*$^{-/-}$ mice might may be maintained by Notch3 signaling.

4.3 Notch signaling is upregulated in P-E- cells

In the canonical Notch pathway, the receptors are cleaved into the Notch extracellular domain (NECD) and Notch intracellular domain (NICD) upon binding their cognate ligands on the contacting cell. The NICD is then translocated into the nucleus and triggers the expression of downstream genes, such as *Hes1* and *Hes5* (Ables et al., 2011). The balance of NSC quiescence and proliferation is regulated by Notch signaling. Its activation causes NSC quiescence, whereas its inhibition reinitiates NSC proliferation and subsequent commitment to neuronal differentiation (Chapouton et al., 2010). The Notch target gene *Hes1* is constitutively expressed in brain compartments that have low proliferation rates and it was shown that ectopic *Hes1* expression reduces proliferation of embryonic neural progenitors *in vitro* (Baek et al., 2006). However, although I observed more qNSCs in the *Tlx*$^{-/-}$ mouse brain with upregulated *Hes1* expression, NICD1 nuclear immunoreactivity was not increased in this cellular subset (Figure 3.5 D). As the NICD1 antibody can only recognize the activated Notch1 but not Notch3, this finding may indicate that Notch1 is not the source of elevated Notch signaling in *Tlx*$^{-/-}$ mice qNSCs. This finding needs further investigation by an antibody specific for Notch3 intracellular domain. However, the treatment with DAPT *in vivo* also indicates that Notch signaling in the mutant niche may be upregulated only in P-E- but not in P+E- cells (Figure 3.10 D). In fact, although blockade of Notch signaling increased proliferation, in both genotypes (Figure 3.9), in the WT this reflects increased total numbers of cycling P+E- and P+E+ cells (Figure 3.10 A and C), whereas in the *Tlx*$^{-/-}$ mice only higher numbers of P+E- and a higher proportion of proliferating P-E- cells (Figure 3.10 B and D). Together with my observation of increased NICD1 immunoreactivity within the population of *Tlx*$^{-/-}$ P-E- cells

(Figure 3.5 E), this suggests the presence of a subset of NSCs included in the P-E- population, which do not express Prominin-1 in the presence of high levels of Notch signalling (Codega et.al 2014, Neuron). Although most of the P-E- cells are neuroblasts, 1.3% of the SVZ cells were clonogenic in neonatal brain (Carrillo-Garcia et al., 2010), which indicated that they are NSCs but Prominin-1 negative. By comparing the gene profile of Notch signaling genes of P-E- cells in *Tlx*$^{-/-}$ with WT, I found that lack of TLX led to an increase of *Hes1* expression levels also in this population (Figure 3.8 A). In fact, this analysis also revealed that the mutation in this subset led also to an increase of *Hes5* expression (Figure 3.8 B). Although there were no significant increase in expression of Notch receptors *Notch1* and *Notch3* in both SVZ regions (Figure 3.8 E and F), the Notch ligand *Dll1* was upregulated in the P-E- cells of the dorsal mutant SVZ (Figure 3.8 D), which may contribute to upregulate basal Notch signaling in these cells. Previous analysis have indicated that Notch signaling represses stem cell properties and proliferation in two main cell groups of adult glial cells: multiciliated ependymal cells (Carlen et al., 2009) and astrocytes in the brain parenchyma (Magnusson et al., 2014). Since no ependymal cells are found in the P-E- cell population (Khatri et al. 2014), it is likely that the P-E- cells represent niche astrocytes that like parenchyma astrocytes display NSC characteristics upon downregulation of Notch signaling. This interpretation is also consistent with the fact that upon DAPT treatment the Ki67 positive cells did not localize in the out layer of ventricle suggesting that they are not ependymal cells (Figure 3.9 A). However, further experiments aimed at characterizing this population will be necessary to confirm this hypothesis.

Since TLX protein may not be expressed in the DCX positive neuroblast cells (Li et al., 2012), which are the main cell types in P-E- cells, and since neuroblasts are less dependent on Notch1 receptor signaling (Albes et al., 2010), it is likely that the increase in *Hes1* and *Hes5* expression in the mutant P-E- cells occurs in the same subset that displays high levels of NICD1 immunoreactivity.

As mentioned above DAPT injection led to an increase in the total amount of P+E+ only in WT but not in *Tlx-/-* mice. A likely explanation of this observation is that in WT, but not in mutant

mice, the increase in the pool of qNSCs leads to a higher number of aNSCs. Thus, TLX promotes the transition between qNSCs to aNSCs by an additional mechanism than the increase in Notch signaling.

4.4 TLX represses Notch target genes in a RBPJ binding site dependent manner

The orphan nuclear receptor TLX (NR2E1) has a DNA binding domain recognizing the conserved sequence (5'-AAGTCA-3') (Mangelsdorf and Evans, 1995). TLX functions as repressor of *Pax2* (Yu et al., 2000), *Pten* (Zhang et al., 2006) and *BMP4* expression (Qin et al 2014). It was shown in the context of genome regulation that TLX can recruit histone deacetylases (HDAC 3 and HDAC5) to the promoters of its target genes, such as *p21* and *Pten* (Sun et al., 2007). Here in my thesis, I showed that the Notch target genes *Hes1* and *Hes5* are also repressed by TLX (Figure 3.12). Moreover, chromatin Immunoprecipitation (ChIP) assays in neurosphere cultures confirmed that the TLX mediated repression was dependent on the RBPJ binding site of the Hes1/5 promoters (Figure 3.13). In classical perspective, RBPJ proteins bind constantly at the promoter of Hes genes (Baolo et al., 2002). Therefore, the repression of *Hes1/5* by TLX may not due to a competitive mechanism with the NICD-RBPJ complex at the DNA binding sequence but instead more dependent on protein-protein interaction with the complex. However recently, Castel et.al showed that the binding of RBPJ to its targets is also inducible and dependents on activation of Notch signaling (Castel et al., 2013).

To investigate the TLX interaction at the RBPJ binding site we used for reporter assays an artificial adenoviral TATA mini promoter with 10 copies of RBPJ binding motifs, which confirmed that overexpression of TLX indeed activated the transcription of RBPJ consensus sequence (Figure 3.12 C and I). This result also highlighted the need of a *Hes1/5* promoter specific repression sequence or other cofactors for the function of TLX as repressor. In addition, cotransfection of NICD1 increased the luciferase activity 6 folds and validated the interaction of NICD at RBPJ binding sites (Figure 3.12 E). Interestingly, the control reporter plasmid without 10 copies of RBPJ binding motifs was also responsive to TLX but not to NICD

overexpression, which suggested that TLX may recruit transcription factors which can interact with the TATA box of the mini promoter.

4.5 P+E- Cells are not clonogenic upon *Hes1* knocking down

The P+E- cells rarely form clones *in vitro*. Only 3.8% P+E- cells from the neonatal SVZ are clonogenic in the presence of EGF and FGF2 (Carrillo-Garcia et al., 2010). And in the adult SVZ, the clone-forming cells reduced to 0.1% (Codega et al., 2014; Khatri et al., 2014). I here did not observed clone formation from P+E- cells, This is likely due to the very strict sorting conditions used here, where only the highly Prominin-1 immunoreactive cells were sorted for clonal analysis, which contains more ependymal cells which do not proliferate (Carlen et al. 2009). Since, it is possible that qNSCs, which display intermediate levels of Prominin-1 immnuoreactivity were not included in the population sorted for the clonogenic assays, whether they can form clones upon *Hes1* downregulation needs to be further investigated. The behavior of P+E- cells upon knocking down of *Hes1* expression needs additionally to be investigated *in vivo*, as the Notch signaling is based on cell-cell contact which is disrupted *in vitro*. However, this analysis is complicated by the difficulty of separately identifying and targeting P+E- and P-E- cells *in vivo*. I found that in the WT adult niche 0.02% cells of the latter can form clones while there is nearly no clone-forming cells in *Tlx*$^{-/-}$ counterpart (Figure 3.14). However, downregulation of Hes1 in this population lead to a conspicuous increase in the mutant but not in the WT genetic background, showing that lack of TLX promotes quiescence in this population by increasing *Hes1* expression. Interestingly, the clonogenic cells mildly decreased in the WT counterpart when knocking down *Hes1*. Since the expression level of *Hes1* is lower in WT than *Tlx*$^{-/-}$, this suggests that the quiescence and proliferation are regulated in a Hes1-dose dependent manner. However, the assumption still needs to be verified.

4.6 Conclusive model of TLX regulates qNSC activation

The TLX protein regulates NSC proliferation and differentiation via repression of effector genes *Hes1* and *Hes5*, thereby affecting Notch signaling, which has been shown very

important for the regulation of NSC behavior in the brain. Indeed, Notch effectors HES1 and HES5 can heterodimerize with bHLH factors such as NGN2 and MASH1 to inhibit neuronal differentiation (Kageyama et al., 2007). In this study, we proposed a model that TLX represses *Hes1* and *Hes5* expression by interacting with RBPJ binding sites at their promoters thereby could release the proneural genes to promote neurogenesis. In the absence of *Tlx*, the increase in *Hes1* expression leads to changes in the expression levels of Notch receptors and ligands, thereby promoting a progressive accumulation of NSCs in a dormant pool, which display high levels of Notch signaling. However, it is still unclear whether upregulation of *Hes1* expression and consequent increase in Notch signaling are also responsible for the impairment in the transition from qNSCs to aNSCs observed in the absence of TLX.

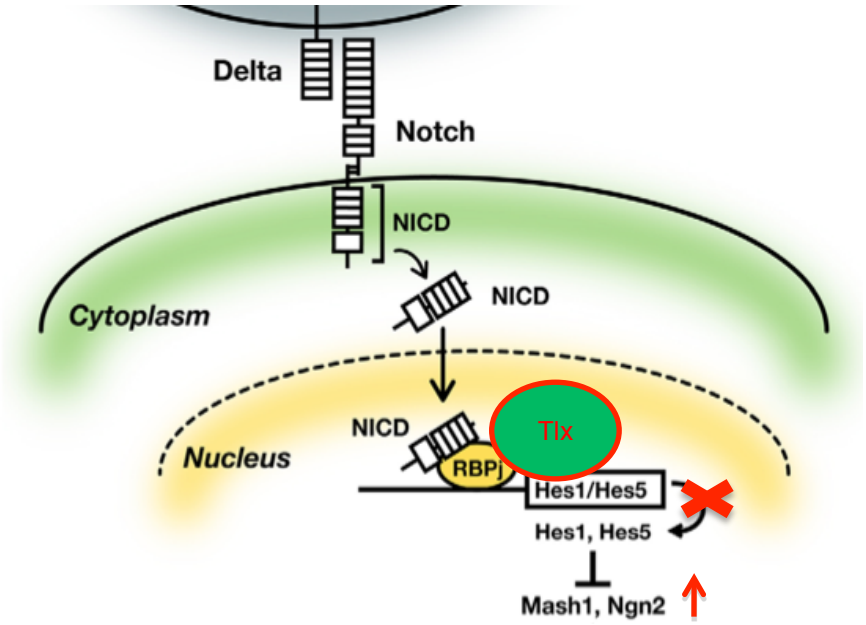

Figure 4.1 Schematic overview of the interaction of Tlx and Notch signaling. Tlx competes with the NICD/RBPJ complex at RBPJ binding sites of *Hes1* and *Hes5* promoters. This release the inhibitory effect of *Hes1/5* on proneural genes *Mash1* and *Ngn2*. (Cartoon adapted from Shimojo et al., 2011 with modification)

4.7 Therapeutic prospect of TLX and neural stem cells

Recently, Zhu et.al demonstrated that brain cancer stem cells are TLX positive and showed that TLX is an indicator for poor survival prognosis of human glioblastoma patients. Therefore, TLX is a promising therapeutic target for the understanding of brain tumor biology (Zhu et al., 2014). Moreover, Benod et.al showed that small compounds can bind to the human TLX

protein and enhance its repressive activity (Benod et al., 2014) underscoring the therapeutic potential of the manipulation of TLX function in cancer stem cells.

Understanding TLX function may have implication also for pathologies other than brain tumours. In fact, induced pluripotent stem cells (iPS) provide a renewable source for the transplantation therapy of the neurological disease. However, the risks such as demanding delicate surgical procedure and graft-induced complications may outweigh the benefits of the transplantation (Yu et al., 2013). Understanding the mechanisms of neural stem cell activation in the adult brain would provide an alternative source of stem cells for the repair of the damaged or injured brain, which could be less invasive.

5. References.

Ables, J.L., Breunig, J.J., Eisch, A.J., and Rakic, P. (2011). Not(ch) just development: Notch signalling in the adult brain. Nat Rev Neurosci *12*, 269-283.

Ables, J.L., DeCarolis, N.A., Johnson, M.A., Rivera, P.D., Gao, Z.L., Cooper, D.C., Radtke, F., Hsieh, J., and Eisch, A.J. (2010). Notch1 Is Required for Maintenance of the Reservoir of Adult Hippocampal Stem Cells. Journal of Neuroscience *30*, 10484-10492.

Alunni, A., Krecsmarik, M., Bosco, A., Galant, S., Pan, L., Moens, C.B., and Bally-Cuif, L. (2013). Notch3 signaling gates cell cycle entry and limits neural stem cell amplification in the adult pallium. Development *140*, 3335-3347.

Alvarez-Buylla, A., and Lois, C. (1995). Neuronal stem cells in the brain of adult vertebrates. STEM CELLS *13*, 263-272.

Andersen, P., Uosaki, H., Shenje, L.T., and Kwon, C. (2012). Non-canonical Notch signaling: emerging role and mechanism. Trends Cell Biol.

Andersson, E.R., Sandberg, R., and Lendahl, U. (2011). Notch signaling: simplicity in design, versatility in function. Development *138*, 3593-3612.

Altman, J. (1962). Are new neurons formed in the brains of adult mammals? Science *135*, 1127-1128.

Baek, J.H., Hatakeyama, J., Sakamoto, S., Ohtsuka, T., and Kageyama, R. (2006). Persistent and high levels of Hes1 expression regulate boundary formation in the developing central nervous system. Development *133*, 2467-2476.

Barolo, S., Stone, T., Bang, A.G., and Posakony, J.W. (2002). Default repression and Notch signaling: Hairless acts as an adaptor to recruit the corepressors Groucho and dCtBP to Suppressor of Hairless. Genes & Development *16*, 1964-1976.

Benod, C., Villagomez, R., Filgueira, C.S., Hwang, P.K., Leonard, P.G., Poncet-Montange, G., Rajagopalan, S., Fletterick, R.J., Gustafsson, J.A., and Webb, P. (2014). The Human Orphan

Nuclear Receptor Tailless (TLX, NR2E1) Is Druggable. Plos One *9*.

Berezovska, O., Xia, M.Q., and Hyman, B.T. (1998). Notch is expressed in adult brain, is coexpressed with presenilin-1, and is altered in Alzheimer disease. J Neuropath Exp Neur *57*, 738-745.

Brummelkamp, T.R., Bernards, R., and Agami, R. (2002). A system for stable expression of short interfering RNAs in mammalian cells. Science *296*, 550-553.

Capela, A., and Temple, S. (2002). LeX/ssea-1 Is Expressed by Adult Mouse CNS Stem Cells, Identifying Them as Nonependymal. Neuron *35*, 11.

Carlen, M., Meletis, K., Goritz, C., Darsalia, V., Evergren, E., Tanigaki, K., Amendola, M., Barnabe-Heider, F., Yeung, M.S., Naldini, L.*, et al.* (2009). Forebrain ependymal cells are Notch-dependent and generate neuroblasts and astrocytes after stroke. Nat Neurosci *12*, 259-267.

Carrillo-Garcia, C., Suh, Y., Obernier, K., Holzl-Wenig, G., Mandl, C., and Ciccolini, F. (2010). Multipotent precursors in the anterior and hippocampal subventricular zone display similar transcription factor signatures but their proliferation and maintenance are differentially regulated. Molecular and cellular neurosciences *44*, 318-329.

Castel, D., Mourikis, P., Bartels, S.J.J., Brinkman, A.B., Tajbakhsh, S., and Stunnenberg, H.G. (2013). Dynamic binding of RBPJ is determined by Notch signaling status. Genes & Development *27*, 1059-1071.

Chapouton, P., Skupien, P., Hesl, B., Coolen, M., Moore, J.C., Madelaine, R., Kremmer, E., Faus-Kessler, T., Blader, P., Lawson, N.D.*, et al.* (2010). Notch Activity Levels Control the Balance between Quiescence and Recruitment of Adult Neural Stem Cells. Journal of Neuroscience *30*, 7961-7974.

Codega, P., Silva-Vargas, V., Paul, A., Maldonado-Soto, A.R., DeLeo, A.M., Pastrana, E., and Doetsch, F. (2014). Prospective Identification and Purification of Quiescent Adult Neural Stem

Cells from Their In Vivo Niche. Neuron *82*, 545-559.

Coskun, V., Wu, H., Blanchi, B., Tsao, S., Kim, K., Zhao, J., Biancotti, J.C., Hutnick, L., Krueger, R.C., Jr., Fan, G.*, et al.* (2008). CD133+ neural stem cells in the ependyma of mammalian postnatal forebrain. Proceedings of the National Academy of Sciences of the United States of America *105*, 1026-1031.

Dang, L., Yoon, K., Wang, M., and Gaiano, N. (2006). Notch3 signaling promotes radial glial/progenitor character in the mammalian telencephalon. Dev Neurosci *28*, 58-69.

de la Pompa, J.L., Wakeham, A., Correia, K.M., Samper, E., Brown, S., Aguilera, R.J., Nakano, T., Honjo, T., Mak, T.W., Rossant, J.*, et al.* (1997). Conservation of the Notch signalling pathway in mammalian neurogenesis. Development *124*, 1139-1148.

Dull, T., Zufferey, R., Kelly, M., Mandel, R.J., Nguyen, M., Trono, D., and Naldini, L. (1998). A third-generation lentivirus vector with a conditional packaging system. Journal of virology *72*, 8463-8471.

Elmi, M., Matsumoto, Y., Zeng, Z.J., Lakshminarasimhan, P., Yang, W., Uemura, A., Nishikawa, S., Moshiri, A., Tajima, N., Agren, H.*, et al.* (2010). TLX activates MASH1 for induction of neuronal lineage commitment of adult hippocampal neuroprogenitors. Molecular and cellular neurosciences *45*, 121-131.

Eriksson, P.S., Perfilieva, E., Bjork-Eriksson, T., Alborn, A.M., Nordborg, C., Peterson, D.A., and Gage, F.H. (1998). Neurogenesis in the adult human hippocampus. Nature medicine *4*, 1313-1317.

Fan, X., Khaki, L., Zhu, T.S., Soules, M.E., Talsma, C.E., Gul, N., Koh, C., Zhang, J., Li, Y.M., Maciaczyk, J.*, et al.* (2010). NOTCH pathway blockade depletes CD133-positive glioblastoma cells and inhibits growth of tumor neurospheres and xenografts. Stem cells *28*, 5-16.

Fischer, J., Beckervordersandforth, R., Tripathi, P., Steiner-Mezzadri, A., Ninkovic, J., and Gotz, M. (2011). Prospective isolation of adult neural stem cells from the mouse

subependymal zone. Nature protocols *6*, 1981-1989.

Guentchev, M., and McKay, R.D. (2006). Notch controls proliferation and differentiation of stem cells in a dose-dependent manner. The European journal of neuroscience *23*, 2289-2296.

Hauck, B., Chen, L., and Xiao, W. (2003). Generation and characterization of chimeric recombinant AAV vectors. Molecular therapy : the journal of the American Society of Gene Therapy *7*, 419-425.

Hirata, H., Yoshiura, S., Ohtsuka, T., Bessho, Y., Harada, T., Yoshikawa, K., and Kageyama, R. (2002). Oscillatory expression of the bHLH factor Hes1 regulated by a negative feedback loop. Science *298*, 840-843.

Ihrie, R.A., and Alvarez-Buylla, A. (2011). Lake-front property: a unique germinal niche by the lateral ventricles of the adult brain. Neuron *70*, 674-686.

Imayoshi, I., Sakamoto, M., and Kageyama, R. (2011). Genetic methods to identify and manipulate newly born neurons in the adult brain. Frontiers in neuroscience *5*, 64.

Johansson, C.B., Momma, S., Clarke, D.L., Risling, M., Lendahl, U., and Frisen, J. (1999). Identification of a neural stem cell in the adult mammalian central nervous system. Cell *96*, 25-34.

Kageyama, R., Ohtsuka, T., and Kobayashi, T. (2007). The Hes gene family: repressors and oscillators that orchestrate embryogenesis. Development *134*, 1243-1251.

Khatri, P., Obernier, K., Simeonova, I.K., Hellwig, A., Holzl-Wenig, G., Mandl, C., Scholl, C., Wolfl, S., Winkler, J., Gaspar, J.A.*, et al.* (2014). Proliferation and cilia dynamics in neural stem cells prospectively isolated from the SEZ. Scientific reports *4*, 3803.

Kobayashi, T., Mizuno, H., Imayoshi, I., Furusawa, C., Shirahige, K., and Kageyama, R. (2009). The cyclic gene Hes1 contributes to diverse differentiation responses of embryonic stem cells. Genes Dev *23*, 1870-1875.

Koch, U., Lehal, R., and Radtke, F. (2013). Stem cells living with a Notch. Development *140*, 689-704.

Kopan, R., and Ilagan, M.X. (2009). The canonical Notch signaling pathway: unfolding the activation mechanism. Cell *137*, 216-233.

Lendahl, U., Zimmerman, L.B., and McKay, R.D. (1990). CNS stem cells express a new class of intermediate filament protein. Cell *60*, 585-595.

Li, S., Sun, G., Murai, K., Ye, P., and Shi, Y. (2012). Characterization of TLX expression in neural stem cells and progenitor cells in adult brains. Plos One *7*, e43324.

Lois, C., Hong, E.J., Pease, S., Brown, E.J., and Baltimore, D. (2002). Germline Transmission and Tissue-Specific Expression of Transgenes Delivered by Lentiviral Vectors. Science *295*, 868-872.

Magnusson, J.P., Goritz, C., Tatarishvili, J., Dias, D.O., Smith, E.M., Lindvall, O., Kokaia, Z., and Frisen, J. (2014). A latent neurogenic program in astrocytes regulated by Notch signaling in the mouse. Science *346*, 237-241.

Mangelsdorf, D.J., and Evans, R.M. (1995). The Rxr Heterodimers and Orphan Receptors. Cell *83*, 841-850.

Mason, H.A., Rakowiecki, S.M., Raftopoulou, M., Nery, S., Huang, Y., Gridley, T., and Fishell, G. (2005). Notch signaling coordinates the patterning of striatal compartments. Development *132*, 4247-4258.

Mckenzie, G., Ward, G., Stallwood, Y., Briend, E., Papadia, S., Lennard, A., Turner, M., Champion, B., and Hardingham, G.E. (2006). Cellular Notch responsiveness is defined by phosphoinositide 3-kinase-dependent signals. Bmc Cell Biol *7*.

Monaghan, A.P., Bock, D., Gass, P., Schwger, A., Wolfer, D.P., Lipp, H.P., and Schutz, G. (1997). Defective limbic system in mice lacking the tailless gene. Nature *390*, 515-517.

Monaghan, A.P., Grau, E., Bock, D., and Schutz, G. (1995). The Mouse Homolog of the Orphan Nuclear Receptor Tailless Is Expressed in the Developing Forebrain. Development *121*, 839-853.

Naldini, L., Blomer, U., Gallay, P., Ory, D., Mulligan, R., Gage, F.H., Verma, I.M., and Trono, D. (1996). In vivo gene delivery and stable transduction of nondividing cells by a lentiviral vector. Science *272*, 263-267.

Nishimura, M., Isaka, F., Ishibashi, M., Tomita, K., Tsuda, H., Nakanishi, S., and Kageyama, R. (1998). Structure, chromosomal locus, and promoter of mouse Hes2 gene, a homologue of Drosophila hairy and Enhancer of split. Genomics *49*, 69-75.

Niu, W., Zou, Y., Shen, C., and Zhang, C.-L. (2011). Activation of Postnatal Neural Stem Cells Requires Nuclear Receptor TLX. The Journal of Neuroscience *31*, 13816-13828.

Obernier, K., Simeonova, I., Fila, T., Mandl, C., Hölzl-Wenig, G., Monaghan-Nichols, P., and Ciccolini, F. (2011). Expression of Tlx in Both Stem Cells and Transit Amplifying Progenitors Regulates Stem Cell Activation and Differentiation in the Neonatal Lateral Subependymal Zone. STEM CELLS *29*, 1415-1426.

Ohtsuka, T., Ishibashi, M., Gradwohl, G., Nakanishi, S., Guillemot, F., and Kageyama, R. (1999). Hes1 and Hes5 as Notch effectors in mammalian neuronal differentiation. Embo Journal *18*, 2196-2207.

Pignoni, F., Baldarelli, R.M., Steingrimsson, E., Diaz, R.J., Patapoutian, A., Merriam, J.R., and Lengyel, J.A. (1990). The Drosophila Gene Tailless Is Expressed at the Embryonic Termini and Is a Member of the Steroid-Receptor Superfamily. Cell *62*, 151-163.

Qin, S., Niu, W., Iqbal, N., Smith, D.K., and Zhang, C.L. (2014). Orphan nuclear receptor TLX regulates astrogenesis by modulating BMP signaling. Frontiers in neuroscience *8*, 74.

Qu, Q., and Shi, Y. (2009). Neural stem cells in the developing and adult brains. J Cell Physiol *221*, 5-9.

Rubinson, D.A., Dillon, C.P., Kwiatkowski, A.V., Sievers, C., Yang, L., Kopinja, J., Rooney, D.L., Zhang, M., Ihrig, M.M., McManus, M.T.*, et al.* (2003). A lentivirus-based system to functionally silence genes in primary mammalian cells, stem cells and transgenic mice by RNA interference. Nature genetics *33*, 401-406.

Ryan, S.M., O'Keeffe, G.W., O'Connor, C., Keeshan, K., and Nolan, Y.M. (2013). Negative regulation of TLX by IL-1beta correlates with an inhibition of adult hippocampal neural precursor cell proliferation. Brain, behavior, and immunity *33*, 7-13.

Shi, Y., Chichung Lie, D., Taupin, P., Nakashima, K., Ray, J., Yu, R.T., Gage, F.H., and Evans, R.M. (2004). Expression and function of orphan nuclear receptor TLX in adult neural stem cells. Nature *427*, 78-83.

Shimojo, H., Ohtsuka, T., and Kageyama, R. (2011). Dynamic expression of notch signaling genes in neural stem/progenitor cells. Frontiers in neuroscience *5*, 78.

Sun, G., Ye, P., Murai, K., Lang, M.-F., Li, S., Zhang, H., Li, W., Fu, C., Yin, J., Wang, A.*, et al.* (2011). miR-137 forms a regulatory loop with nuclear receptor TLX and LSD1 in neural stem cells. Nat Commun *2*, 529.

Sun, G., Yu, R.T., Evans, R.M., and Shi, Y. (2007). Orphan nuclear receptor TLX recruits histone deacetylases to repress transcription and regulate neural stem cell proliferation. Proceedings of the National Academy of Sciences of the United States of America *104*, 15282-15287.

Walker, T.L., Wierick, A., Sykes, A.M., Waldau, B., Corbeil, D., Carmeliet, P., and Kempermann, G. (2013). Prominin-1 Allows Prospective Isolation of Neural Stem Cells from the Adult Murine Hippocampus. J Neurosci *33*, 3010-3024.

Wang, J., Sakariassen, P.O., Tsinkalovsky, O., Immervoll, H., Boe, S.O., Svendsen, A., Prestegarden, L., Rosland, G., Thorsen, F., Stuhr, L.*, et al.* (2008). CD133 negative glioma cells form tumors in nude rats and give rise to CD133 positive cells. Int J Cancer *122*, 761-768.

Young, K.M., Fogarty, M., Kessaris, N., and Richardson, W.D. (2007). Subventricular zone stem cells are heterogeneous with respect to their embryonic origins and neurogenic fates in the adult olfactory bulb. Journal of Neuroscience *27*, 8286-8296.

Yu, R.T., Chiang, M.Y., Tanabe, T., Kobayashi, M., Yasuda, K., Evans, R.M., and Umesono, K. (2000). The orphan nuclear receptor Tlx regulates Pax2 and is essential for vision. Proceedings of the National Academy of Sciences of the United States of America *97*, 2621-2625.

Yu, R.T., Mckeown, M., Evans, R.M., and Umesono, K. (1994). Relationship between Drosophila Gap Gene Tailless and a Vertebrate Nuclear Receptor Tlx. Nature *370*, 375-379.

Yu, X., Alder, J.K., Chun, J.H., Friedman, A.D., Heimfeld, S., Cheng, L., and Civin, C.I. (2006). HES1 inhibits cycling of hematopoietic progenitor cells via DNA binding. STEM CELLS *24*, 876-888.

Zhang, C.L., Zou, Y., Yu, R.T., Gage, F.H., and Evans, R.M. (2006). Nuclear receptor TLX prevents retinal dystrophy and recruits the corepressor atrophin1. Genes Dev *20*, 1308-1320.

Zhao, C., Sun, G., Li, S., Lang, M.-F., Yang, S., Li, W., and Shi, Y. (2010). MicroRNA let-7b regulates neural stem cell proliferation and differentiation by targeting nuclear receptor TLX signaling. Proceedings of the National Academy of Sciences *107*, 1876-1881.

Zhao, C., Sun, G., Li, S., and Shi, Y. (2009). A feedback regulatory loop involving microRNA-9 and nuclear receptor TLX in neural stem cell fate determination. Nat Struct Mol Biol *16*, 365-371.

Zhao, C., Sun, G., Ye, P., Li, S., and Shi, Y. (2013). MicroRNA let-7d regulates the TLX/microRNA-9 cascade to control neural cell fate and neurogenesis. Scientific reports *3*, 1329.

Zhu, Z., Khan, M.A., Weiler, M., Blaes, J., Jestaedt, L., Geibert, M., Zou, P., Gronych, J., Bernhardt, O., Korshunov, A.*, et al.* (2014). Targeting Self-Renewal in High-Grade Brain

Tumors Leads to Loss of Brain Tumor Stem Cells and Prolonged Survival. Cell Stem Cell.

Zufferey, R., Nagy, D., Mandel, R.J., Naldini, L., and Trono, D. (1997). Multiply attenuated lentiviral vector achieves efficient gene delivery in vivo. Nature biotechnology *15*, 871-87

6. Abbreviations:

aNSC	Activated Neural Stem Cells
b-gal	Beta-galactosidase
bHLH	Basic helix-loop-helix
BMP	Bone morphogenetic protein
bp	Base pair
BrdU	5-bromo-2-deoxyuridine
Bv	Blood vessel
ChIP	Chromatin immunoprecipitation
CNS	Central nervous system
CSF	Cerebrospinal fluid
DAPI	4', 6-diamidino-2-phenylindole
DAPT	N-[N-(3,5-Difluorophenacetyl)-L-alanyl]-S-phenylglycine t-butyl ester
DCX	Doublecortin
DG	Dentate gyrus
DIV	Day in vitro
Dll	Delta-like
EGF	Epidermal growth factor
EGFR	Epidermal growth factor receptor
FACS	Fluorescence activated cell sorting
FCS	Fetal calf serum
FGF	Fibroblast growth factor
GFAP	Glial fibrillary acidic protein
H	Hour

HDAC	Histone deacetylase complex
Hes1/5	Hairy and enhancer of split-1/5
KO	Knock out
LV	Lateral ventricle
Min	Minute
Mash1 (Ascl1)	Mammalian achaete-schute homolog 1
NICD	Notch intercellular domain
NSC	Neural stem cell
NPC	Neural progenitor cell
OB	Olfactory bulb
PBS	Phosphate buffered saline
PCR	Polymerase chain reaction
PFA	Paraformaldehyde
PI	Propidium iodide
PIC	Protease Inhibitor Cocktail II
qNSC	Quiescent neural stem cell
RBPJ	Recombining binding protein suppressor of hairless
RMS	Rostral migration stream
RG	Radial glia cell
RT-PCR	Real time-PCR
S	Second
SGZ	Subgranular zone
SVZ	Subventricular zone
SEZ	Subependymal zone
TAPs	Transit amplifying cells

Tlx (Tll)	Tailless
UTR	Untranslated region
WT	Wild type

7. Acknowledgements

Science is long and time is fleeting. It has been three years since I started my PhD study here in the beautiful city-Heidelberg. And now I have to write the final part of my thesis. Every moments in the last three years flashed by my mind's eye and it was not an easy three-year in my life. And I could not help being so sentimental when I am trying to recall all those moments. However, life could be much harder without all your help. I would like to express my sincere gratitude to all those who offered me the possibility to start and complete this thesis.

First of all, I would like to express many thanks to my supervisor, Dr. Francesca Ciccolini for her great support, thoughtful guidance and intensive discussions for my PhD study. Without her, I may not start my PhD study in Heidelberg three years ago. And without her, I may not complete my PhD study now. I also thank to all my group members. It would be impossible to finish this thesis without their generous help. In particular, I would like to thank Gaby Hölzl-Wenig for helping me with the FACS experiments and also for the helpful discussions. I would thank Claudia Mandl for introducing me the right way to do dissection, immunohistochemistry and stereotaxic surgery and many important experiments in my thesis. And I would like to thank Yuting Li, Ina Simeonova, Priti Khatri and Udo Schmidt-Edelkraut for their kind discussions for the experiments and also friendship.

I would also like to express many thanks to Prof. Dr. Hilmar Bading and Prof. Dr. Ulrike Müller for supervising this dissertation. Thanks for all their constructive advices and suggestions. I thank all the friends and colleagues in the Bading group. Especially I would like to express many thanks to Otto Bräunling and Irmela Meng for all their supports of the daily life in and out the lab. Thanks to Yan Yu, Yanwei Tan, Peter Bengtson and Priit Pruunsild for discussing the technique details and tricks of experiments. Thanks to Ursula Weiss, Andrea Hellwig, Monika Keusch, Oliver Teubner and Alan Summerfield for their excellent job for supporting my work in the lab.

I could not forget to thank the Baden-Württemberg Stiftung for their generous funding. And I have to thank HBIGS (Hartmut Hoffmann-Berling International Graduate School of Molecular

and Cellular Biology) for providing me the opportunity to do my PhD study here. Besides, I have to thank HBIGS for supporting my family. Without their support, my son could not grow up happily in the daycare center.

And last but not least, I thank my family for their accompany and endless love. Without them I would not be able to study abroad and finish this thesis work. I deeply express my gratitude to my wife, Ting for her love and encouragement and emotional support that makes me survive in Germany. And also to my son who makes my life more colorful. I also thank my parents for loving me and supporting me since the day I was born.

8. List of Figures